Snow water equivalents exclusively from snow depths and their temporal changes: The ΔSNOW model

Michael Winkler[1,*], Harald Schellander[1,2,*], and Stefanie Gruber[1]

[1]ZAMG – Zentralanstalt für Meteorologie und Geodynamik, Innsbruck, Austria
[2]Department of Atmospheric and Cryospheric Sciences, University of Innsbruck, Austria
[*]These authors contributed equally to this work.

Correspondence: Michael Winkler (michael.winkler@zamg.ac.at) and Harald Schellander (harald.schellander@zamg.ac.at)

Abstract. Reliable historical manual measurements of snow depths are available for many years, sometimes decades, across the globe, and increasingly snow depth data is also available from automatic stations and remote sensing platforms. In contrast, records of snow water equivalent (SWE) are sparse, which is significant as SWE is commonly the most important snowpack feature for hydrology, climatology, agriculture, natural hazards and other fields.

Existing methods of modeling SWE either rely on detailed meteorological forcing being available or are not intended to simulate individual SWE values, such as seasonal "peak SWE". Here we present a new semi-empirical multi-layer model, ΔSNOW, for simulating SWE and bulk snow density solely from a regular time series of snow depths. The model, which is freely available as an R-package, treats snow compaction following the rules of Newtonian viscosity, considers errors in measured snow depth, treats overburden loads due to new snow as additional unsteady compaction, and if snow is melted, the water mass is stepwise distributed top-down in the snowpack. Seven model parameters are subject to calibration.

Snow observations of 67 winters from 14 stations, well-distributed over different altitudes and climatic regions of the Alps, are used to find an optimal parameter setting. Data from another 71 independent winters from 15 stations is used for validation. Results are very promising: Median bias and root mean square error for SWE are only $-3.0\,\mathrm{kg\,m^{-2}}$ and $30.8\,\mathrm{kg\,m^{-2}}$, and $+0.3\,\mathrm{kg\,m^{-2}}$ and $36.3\,\mathrm{kg\,m^{-2}}$ for peak SWE, respectively. This is a major advance compared to snow models relying on empirical regressions and even sophisticated thermodynamic snow models do not necessarily perform better. As such the new model offers a means to derive robust SWE estimates from historical snow depth data and, with some modification, to generate distributed SWE from remotely sensed estimates of spatial snow depth distribution.

1 Introduction

Depth (HS) and bulk density (ρ_b) are fundamental characteristics of a seasonal snowpack (e.g., Goodison et al., 1981; Fierz et al., 2009). Their product yields~~Equation (1) links them to~~ the areal density $[\mathrm{kg\,m^{-2}}]$ of the snowpack, which is often~~ in~~

~~hydrological applications – is usually~~ referred to as snow water equivalent (SWE)~~, as it resembles "the depth of water that would result if the mass of snow melted completely" (Fierz et al., 2009).~~[1]

$$SWE = HS \cdot \rho_{\mathrm{b}}$$
$$\underline{[1\,\mathrm{kg\,m^{-2}} \equiv 1\,\mathrm{mm\,water\,equivalent\,(w.e.)}]}$$

(1)

Water resource management, agricultural applications, hydrological modeling, climate analyses, natural hazard assessments,
and many other fields~~Many hydrological, agricultural, and other applications~~ depend on good estimates of SWE~~(e.g., Goodison et al. (1981); Sturm and Holmgred (1998). T~~Ultimately, ~~t~~he mass of water stored in the snowpacks is often more relevant than ~~the~~ snow depth. Particularly~~, especially~~ seasonal SWE maxima, i.e. "peak SWE" (SWE_{pk})~~, . SWE_{\mathrm{pk}}~~ is required for, e.g., discharge or flood forecasting as well as analyses of climate and extremes. The latter, in turn,~~extreme value and climatic analyses, both of which~~ rely on longterm or "historical" data. ~~For example, snow load standards (e.g., International Organization for Standardization, 2013) rely on extreme value analyses of longterm SWE records, as snow load is defined as the product of SWE and the gravitational acceleration.~~ While measurements of HS are relatively widely available, the more useful value of SWE is more difficult to determine and is consequently relatively poorly known, hampering efforts to understand SWE variance and related vast management practices. To address this limitation this paper focuses on developing a robust method to derive SWE from more readily available and historical records of HS.

1.1 Measurements of HS and SWE

Measuring HS is relatively easy (e.g., Sturm and Holmgren, 1998): Manual measurements at a certain point only require a rod or ruler (e.g., Kinar and Pomeroy, 2015), and decades-long series of daily HS measurements exist in many regions – both lowlands and alpine areas (e.g., Haberkorn, 2019). More recently, automatic measurements of HS (mostly sonic or laser distance ranging) have become available, typically with sub-hourly resolution (McCreight and Small, 2014), and remotely sensed HS vastly expands on the areal coverage of manual measurements, although in most cases at the cost of accuracy, temporal resolution and regularity. (Dietz et al. (2012) give a general review of remotely sensed HS measurements, and Painter et al. (2016) provide a thorough overview. Deems et al. (2013) review lidar measurements of HS, while Garvelmann et al. (2013) and Parajka et al. (2012) illustrate the potential of timelapse photography.)

In contrast, measurements of SWE (or ρ_{b}) are more difficult (e.g., Sturm et al., 2010): Manual measurements are time consuming, and require some skill and basic equipment like snow tubes or snow sampling cylinders. For most snowpacks a pit has to be dug to consider the layered structure of the snowpack (e.g., Kinar and Pomeroy, 2015). As a consequence, SWE measurements are much more sparse than HS measurements (e.g., Mizukami and Perica, 2008; Sturm et al., 2010), their accuracy is lower, and time series are shorter. Only in very rare cases are consecutive, decades-long measurement series available (e.g., in Switzerland; cf. Jonas et al., 2009). Even for regularly measured "snow courses", data is sporadic in time and rarely more than biweekly. Also automatic measurements of SWE are not at all comparable in quality and quantity with

---

[1]Equation (1) was deleted during the revision.

automated HS measurements. They are quite expensive, often inaccurate, still at a developmental stage, and/or suffer from significant problems if not intensively maintained throughout the snowy season. Methods involve weighing techniques (snow scales; e.g., Smith et al., 2017; Johnson et al., 2015), pressure measurements (snow pillows; e.g., Goodison et al., 1981), upward-looking ground penetrating radar (e.g., Heilig et al., 2009), passive gamma radiation (e.g., Smith et al., 2017), cosmic ray neutron sensing (e.g., Schattan et al., 2019), L-band Global Navigation Satellite Signals (e.g., Koch et al., 2019), the biggest and best serviced network of automated SWE measurements most likely is SNOTEL with about 800 sites in Western North America (Avanzi et al., 2015).

Remotely sensed SWE data are not operationally available for the local and point scale, and deriving this snow property from satellite products at sub-kilometer resolution is still not possible (Smyth et al., 2019). Furthermore, the available automated measurements and rough estimates of SWE remote sensing instruments are only available for some twenty years at best (e.g., SNOTEL, operated since the late 1990s), which is short compared to decades-long daily HS data (e.g., Kinar and Pomeroy, 2015).

1.2 Modeling SWE

1.2.1 Thermodynamic snow models

Modern snow models such as Crocus (e.g., Vionnet et al., 2012), SNOWPACK (e.g., Lehning et al., 2002), SNTHERM (Jordan, 1991), or the dual-layer model SNOBAL (Marks et al., 1998) resolve mass and energy exchanges within the ground-snow-atmosphere regime in a detailed way by depicting the layered structure of seasonal snowpacks. Echoing Langlois et al. (2009), these models, that comprise all energy balance and temperature index models, will be termed "thermodynamic snow models" hereafter. They all need atmospheric variables as input, primarily precipitation, temperature, humidity, wind speed, and radiative fluxes, and even simplified variants require temperature and/or precipitation (e.g., De Michele et al., 2013) or climatological means thereof (Hill et al., 2019). Avanzi et al. (2015) provide a good review. Unfortunately, many valuable longterm HS series do not have accompanying data required to force a thermodynamic snow model for calculating the associated SWE, and parametrizing or downscaling forcing data from other sources in turn is susceptible to errors. Thermodynamic snow models are typically able to simulate snowpack features beyond SWE and bulk snow density (e.g., grain types, energy fluxes, stabilities etc.), but they are not applicable to derive SWE exclusively from HS.

1.2.2 Empirical regression models

Statistical models of SWE derived from HS and a combination of date, altitude and regional parameters (like Guyennon et al., 2019; Pistocchi, 2016; Gruber, 2014; Mizukami and Perica, 2008; Jonas et al., 2009) are hereafter termed "empirical regression models" (ERMs), and a listing of existing approaches is given in Avanzi et al. (2015). ERMs rely on the strong, near-linear dependence between HS and SWE (cf., e.g., Jonas et al., 2009). According to Gruber (2014) and Valt et al. (2018) HS describes 81% and 85% of SWE variance, respectively. This behavior is based on the narrow range within which the majority

of bulk snow densities lie, and leads to the well-known characteristic of HS–SWE–ρ_b datasets: log-normally distributed HS and SWE and normally distributed ρ_b (e.g., Sturm et al., 2010).

In most ERMs absolute, single-day HS observations are the only snow characteristics used. Depending on calibration focus they can usually only adequately model single SWE features (e.g. mean-SWE or SWE_pk, mid winter or spring). For example, those calibrated for good estimates of mean-SWE fail to model SWE_pk sufficiently well, those designed for SWE_pk often give poor SWE results during phases with shallow snowpacks. Typically, they simulate unrealistic mass losses during phases with compaction only by metamorphism and deformation. The timing of SWE_pk as well as the duration of high snow loads cannot be modeled well. As stated by Jonas et al. (2009) those models cannot be used to "convert time series of HS into SWE at daily resolution or higher" because they may "feature an incorrect fine structure in the temporal course of SWE". Therefore, ERMs are not suitable to calculate SWE for individual days.

McCreight and Small (2014) not only use single-day HS values for their regression model, but also the "evolution" of daily HS. They make use of the negative correlation of HS and ρ_b at short timescales and their positive/negative correlation at longer timescales during accumulation/ablation phases. This development is limited by the fact that the model parameters can only be estimated through regressions relying on "at least three" training datasets of HS and ρ_b from nearby stations. This disqualifies the model of McCreight and Small (2014) for assigning SWE to longterm and historical HS series as consecutive SWE measurements are not available.

1.2.3 Semi-empirical models

An alternative approach that links HS and SWE throughout a snowy season without the need of further meteorological input is provided by Martinec (1977) and revisited by Martinec and Rango (1991): They use a method already developed by Martinec (1956) "to compute the water equivalent from daily total depths of the seasonal snow cover". Snow compaction is expressed as a time-dependent power function. Each layer's snow density ρ_n after n days is given by $\rho_n = \rho_0 \cdot (n+1)^{0.3}$, where ρ_0 is the initial density of the snow layer. Martinec and Rango (1991) set ρ_0 to $100\,\mathrm{kg\,m^{-3}}$, Martinec (1977) varied it from 80 to $120\,\mathrm{kg\,m^{-3}}$. This computation is meant to give good results for the seasonal maximum snow water equivalent (SWE_pk). It is shown, the older the snow the less important is the correct choice of the crucial parameter ρ_0 (Martinec, 1977; Martinec and Rango, 1991). Their model interprets "each increase of total snow depth [...] as snow fall" and if "the total snow depth remains higher than the settling by [the power function], this is also interpreted as new snow. If the snow depth drops lower than the value of the superimposed settling curve of the respective snow layers, it is interpreted as snowmelt, and a corresponding water equivalent is subtracted. In this way the water equivalent of the snow cover can be continuously simulated [...]" (Martinec and Rango, 1991). Rohrer and Braun (1994) improved this model particularly for the ablation season by further increasing density whenever melt conditions are modelled and by introducing a maximum possible snow density of $450\,\mathrm{kg\,m^{-3}}$.

Semi-empirical snow models simulate individual snowpack layers and make use of simple densification concepts. (Hence they are not "fully" empirical.) They cannot model snow properties aside from SWE and density, but their only required input is a HS record: No forcing by atmospheric conditions is needed. In some respects these models bridge the gap between thermodynamic models and ERMs.

1.3 Motivation for a new approach

Table 1 summarizes the classification of SWE models with respect to their essential input. Given the strong need for robust SWE data for numerous applications, and the combined simplicity and effectiveness of semi-empirical models, it is notable that this type of model has received little attention in recent years. Here we focus on developing a robust semi-empirical model
120   that can be used to capitalize on more widespread modern day HS data, as well as to derive SWE from historical HS records.

The semi-empirical method of determining SWE presented here maintains the key feature of previous semi-empirical models considering only the change of snow depth as a proxy for the various processes altering bulk snow density and snow water equivalent, but further

- bases its (dry) snow densification function on Newtonian viscosity,

125   - provides a way to deal with small discrepancies between model and observation (in the order of HS measurement errors),

- takes into account unsteady compaction of underlying, older snow layers due to overburden snow loads, and

- densifies snow layers from top to bottom during melting phases without automatically modeling mass loss due to runoff.

The ideas for the latter three advancements are taken from Gruber (2014), who described them but did not suitably include them as a model. The new modeling approach is named ΔSNOW. Its code is available as *niXmass* package in R (R Core Team,
130   2019), which also includes other models that use snow depth and its temporal change (*nix*...Latin for "snow") to simulate SWE (i.e., snow *mass*).

2 Method

Snow compacts over time due to various processes. Jordan et al. (2010) categorize them in snow drift, dry and wet metamorphism, and deformation. The ΔSNOW model cannot deal with snow drift, however, it differentiates between the latter processes.
135   Table 2 shows the processes modelled and their corresponding ΔSNOW modules and outlines the processes that are ignored. The specific modules are described in Sects. 2.1 and 2.2, a schematic of the model is shown in Fig. 1.

2.0.1 Preliminary: the first snow layer

For non-zero snow depth observations ($HS_{\mathrm{obs}} > 0$) after a snow-free period the following features are assigned to the ΔSNOW model snowpack: There is one snow layer ($ly = 1$). Thickness of this model layer (hs) and total model snow depth (HS) are
140   equal, and set to observed snow depth: $hs = HS := HS_{\mathrm{obs}}$. Analogously, the layer's snow water equivalent equals total snow water equivalent: $swe = SWE := \rho_0 \cdot HS_{\mathrm{obs}}$, with new snow density ρ_0 being an important parameter of the ΔSNOW model (cf. Sect. 3). The treatment of the first snow event is illustrated at $t = 2$ in Fig. 1.

2.1 Dry compaction module

Martinec and Rango (1991) used a power function to describe densification of aging snow, because this way errors in initial density ρ_0 become less relevant over time. As ΔSNOW also aims to robustly model SWE of ephemeral snowpacks (e.g., at low elevation sites) and as overburden load is considered in a particular way (Sect. 2.2.1), it is not expedient to have a direct dependence between density and age of a layer. Instead of a power law, ΔSNOW (like most modern snow models) simulates snow compaction by way of Newtonian viscosity with associated exponential densification over time (e.g., Jordan et al., 2010). In the *Dry Compaction module* the densifying effects of dry metamorphism and deformation are combined, by adopting the relations of Sturm and Holmgren (1998) and De Michele et al. (2013):

$$\frac{hs(i,t-1)}{hs(i,t)} = 1 + \Delta t \cdot \frac{\widehat{\sigma}(i,t)}{\eta(i,t)}$$

$$\text{with } \widehat{\sigma}(i,t) = g \cdot \sum_{\hat{i}=i}^{ly(t)} swe(\hat{i},t) \tag{2}$$

$$\text{and } \eta(i,t) = \eta_0 \cdot e^{k \cdot \rho(i,t)}$$

t and $t-1$ are the points in time of the actual and the preceding snow depth observation, respectively. The timespan between these measurements is Δt, which is in general arbitrary, but usually it is taken to be one day. $hs(i,t)$ is the actual modeled thickness of the i-th snow layer. The actual depth of the total snowpack is $HS(t) = \sum_i hs(i,t)$.

The individual snow water equivalents of the layers are given by $swe(i,t)$, and their sum represents total mass of the snowpack $SWE(t) = \sum_i swe(i,t)$. The vertical stress at the bottom of layer i is given by $\widehat{\sigma}(i,t)$ (De Michele et al., 2013). It is induced by the sum of loads overlying layer i, with $ly(t)$ being the total number of snow layers.

The Newtonian viscosity of snow η is made density-dependent in the framework of the ΔSNOW model (following Kojima, 1967), but dependencies on temperature, or grain characteristics are consciously ignored – due to the lack of information on it when dealing with pure snow depth data. The actual density of layer i is $\rho(i,t)$; it equals $\frac{swe(i,t)}{hs(i,t)}$. k and η_0 are tuning parameters of the *Dry Compaction module* (see Sect. 3).

To avoid excessive compaction a crucial parameter is introduced in ΔSNOW, as was done by Rohrer and Braun (1994): ρ_{max}. It defines the maximal possible density of a snow layer and, consequently, also the maximum bulk snow density. Finding its optimal value for ΔSNOW is subject to calibration (Sect. 2.3).

According to Eq. (2) the rate of densification of a certain snow layer is linearly dependent on the overlying snow load $\widehat{\sigma}(i,t)$ and exponentially dependent on the layer's density $\rho(i,t)$. Sturm and Holmgren (1998) conclude that this difference is one reason why "snow load plays a more limited role in determining the compaction behavior than grain and bond characteristics and temperature". Equation (2) links the densification rate to the layer age, but indirectly by the use of density, and not directly as it was the case with Martinec and Rango (1991)'s power law approach. Consequently, ΔSNOW's compaction is not directly dependent on layer age, which is a prerequisite for the functioning of the *Overburden submodule* (Sect. 2.2.1).

The *Dry Compaction module* is illustrated by the light blue arrows in Fig. 1. This module is applied at every point in time (except if there is no snow; see $t = 1$ in Fig. 1). It is the core module as its output determines the subsequent process decisions, and which module will be applied.

2.2 Process decisions

175   At every point in time, after the *Dry Compaction module* is run, observed $HS_{\text{obs}}(t)$ and modeled $HS(t)$ are compared. The ΔSNOW's process decision algorithm confronts the difference $\Delta HS(t) = HS_{\text{obs}}(t) - HS(t)$ with τ [m]. τ is another tuning parameter of ΔSNOW (see Sect. 2.3). Technically, τ is a threshold deviation and defines a limit of $\Delta HS(t)$ whose overshooting, adherence, and undershooting heads for one out of the modules described in the following Sects. 2.2.1 to 2.2.3. Table 2 links them to snow physics.

180   ### 2.2.1 New snow module

In case $\Delta HS(t) > +\tau$, meaning observed snow depth is significantly higher than modeled snow depth, a new snow event is assumed to have occurred and a new top snow layer is modeled (see at $t = 2$ and $t = 7$ in Fig. 1). Other models have implemented this mechanism (e.g., Martinec and Rango, 1991; Sturm et al., 2010). However, ΔSNOW goes further and explicitly models the effect of overburden load on underlying layers, defined as their enhanced densification due to stress, which is applied by

185   the weight of new snow. Grain bonds get broken, grains slide, partially melt, and warp (Jordan et al., 2010), and the layers densify comparatively rapidly and strongly. ΔSNOW interprets overburden load as an "unsteady and discontinuous" stress on the snowpack, under which snow presumably does not react as a viscous Newtonian fluid. As long as the time between two consecutive observations Δt is in the order of at least some hours, discontinuity is an intrinsic feature of the process.

The *New Snow module* realizes the effect of overburden load through the *Overburden submodule* by reducing each layer's

190   thickness $hs(i,t)$ using the dimensionless "overburden strain" $\epsilon(i,t)$, defined as

$$\epsilon(i,t) = c_{\text{ov}} \cdot \sigma_0 \cdot e^{-k_{\text{ov}} \frac{\rho(i,t)}{\rho_{\max} - \rho(i,t)}}$$

$$\text{with } \sigma_0 = \Delta HS(t) \cdot \rho_0 \cdot g. \tag{3}$$

c_{ov} [Pa^{-1}] is another tuning parameter of the model (see Sect. 2.3) and controls the importance of the unsteady compaction due to overburden load. According to Sturm and Holmgren (1998) and in consistency with Eq. (2) snow load has a linear effect on the bulk density. Therefore, $\epsilon(i,t)$ is a linear function depending on the load, applied by the overlying new snow on the

195   underlying layers. This load is well approximated by σ_0 [Pa]; the larger the overburden load, the stronger the compaction. (The overburden load does not fully equal σ_0, since $\Delta HS(t)$ is not the depth of the new snow, but the difference between modeled depth "before" knowing about the new snow event and observed depth "after" the new snow event. An iterative calculation would be more precise, however, Eq. (3) proved to be an adequate compromise between simplicity and accuracy.) In order to avoid $\epsilon(i,t) > 1$, c_{ov} is restricted at least to the range of values between 0 and the minimum value of the data record

200   for $\frac{1}{\sigma_0}$. As σ_0 hardly ever exceeds $1000 \, \text{Pa}$, $\frac{1}{\sigma_0}$ normally is larger than $1 \times 10^{-3} \, \text{Pa}^{-1}$. This value marks an upper bound for c_{ov}

(Sect. 2.3). Dimensionless k_{ov} controls the role of a certain snow layer's density on $\epsilon(i,t)$, and has to be specified by calibration (see Sect. 2.3). The density-dependence of $\epsilon(i,t)$ was chosen to be exponential, and is constrained by ρ_{max}.

The "overburden strain" $\epsilon(i,t)$ theoretically lies between 0 and 1 and compresses all snow layers of the model in case of a new snow event. Practically, $\epsilon(i,t)$ is often close to zero (in this study 90% of all computed ϵ are smaller than 0.09) and extremely rarely higher than 0.3 (in this study only 9 out of 10000).

The intermediate snow layer thicknesses are $hs^*(i,t) = (1 - \epsilon(i,t)) \cdot hs(i,t)$ and $HS^*(t) = \sum_i hs^*(i,t)$. The compressed layer's masses, $swe(i,t)$, remain unaffected during this process. A new snow event, identified by the condition $\Delta HS(t) > +\tau$, of course not only impacts the older snow and compacts it more strongly, but it also adds a new snow layer and mass to the snowpack (pink arrow at $t = 2$ and $t = 7$ in Fig. 1). The following attributes are given to the new layer $hs(ly,t) = HS_{obs}(t) - HS^*(t)$ and $swe(ly,t) = hs(ly,t) \cdot \rho_0$, and the total snow water equivalent is risen, $SWE(i,t) = SWE(i,t-1) + swe(ly,t)$. The model-snowpack with its new properties subsequently is compacted according to Eq. (2) and the process decision starts again as described in Sect. 2.2. The *Overburden submodule* is illustrated with a purple arrow at $t = 7$ in Fig. 1.

2.2.2 Scaling module

Equations (2) and (3) are highly simplified representations of the complex viscoelastic behavior of snow, and available HS observations typically only show an accuracy of a few centimeters. The ΔSNOW model accepts these inherent inaccuracies by not applying too strict criteria in the process decisions described in Sect. 2.2. The threshold deviation τ acts as a buffer to avoid too frequent gain or loss of mass: In case $|\Delta HS| \leq |\tau|$ neither the snowpack looses mass nor gains mass, but mass is kept constant. In order to benefit from having a new measurement at every point in time, $HS(t)$ is intentionally set to $HS_{obs}(t)$ by the *Scaling module*.

The *Scaling module* forces a partial revaluation of the previous compaction, which was modeled by the *Dry Compaction module* between $t-1$ and t. The best-fitted parameter setting for η_0 is temporarily rejected and substituted by η_0^*. It would be straightforward to use one adjusted $\eta_0^*(t)$ for all layers. However, this leads to multiple solutions for $\eta_0^*(t)$, making it necessary to calculate different $\eta_0^*(i,t)$ for each layer i. See Appendix B for details on that.

$\eta_0^*(i,t)$ is then used instead of η_0 in Eq. (2) to recalculate the compaction of individual layers. $HS(t)$ now equals $HS_{obs}(t)$. In most cases all layers get "slightly more" or "slightly less" compacted by the *Scaling module* than by the *Dry Compaction module*. Only at rare occasions the scaling does not lead to a compaction, but to a small "stretching" of the snowpack. This only happens if there was a small increase in observed snow depth and very little modeled dry metamorphic compaction; the condition $HS(t) + \tau > HS_{obs}(t) > HS_{obs}(t-1)$ has to be fulfilled. Of course, such "stretching" does not occur in reality, but also in the model it occurs only rarely and at small scale: in any case the "stretching" is smaller than τ. The issue is accepted as a model artifact, not least, because the "stretching" enables the very valuable adjustment to HS_{obs} at every point in time without forcing mass gains for insignificant HS raises within the measurement accuracy.

In case the density of an individual layer exceeds ρ_{max} by the scaling process, the excess mass is distributed layerwise from top to bottom. SWE remains constant during scaling, unless it would be necessary to compact all layers beyond ρ_{max}. In this case the appropriate excess mass is taken from the model-snowpack and interpreted as runoff, SWE is reduced and all layer

thicknesses are cut accordingly (see *Runoff submodule* in Sect. 2.2.3 for details). As τ turns out to be reasonably chosen in the order of a few centimeters by calibration (Sect. 3), the resulting reduction of SWE within the *Scaling module* is always quite small: e.g., with $\tau = 2\,\mathrm{cm}$ and maximum density chosen $450\,\mathrm{kg\,m^{-3}}$ (like Rohrer and Braun, 1994) the mass loss due to runoff is only $9\,\mathrm{kg\,m^{-2}}$.

The *Scaling module* is illustrated as black arrows in Fig. 1. Note, the scaling is nothing "physical", but also nothing "substantial" in terms of SWE, yet it is a way to utilize the advantage of having a measured snow depth at every point in time.

2.2.3 Drenching module

The *Drenching module* simulates compaction due to liquid water percolating from top to bottom through the snowpack, loosening grain bonds and leading to densification (wet snow metamorphism). In case observed snow depth at a certain point in time is significantly lower than modeled snow depth ($\Delta HS(t) < -\tau$), the *Drenching module* is activated.

ΔSNOW ignores rain on snow since it concentrates on modeling SWE for pure snow depth records without having any further information on e.g precipitation, temperature, snowfall level, etc. Possibilities of how rain could be addressed in future developments are outlined in Sect. 4.6.

To cope with the model-observation-discrepancy $\Delta HS(t) < -\tau$ the *Drenching module* densifies the model layers until ρ_{max} is reached, starting from the uppermost one. Figuratively spoken, a certain layer gets drenched until saturation and meltwater is further distributed to the underlying layer. This process is repeated until transient HS^* equals $HS_{\mathrm{obs}}(t)$. One or more layers might reach ρ_{max}. In case $\Delta HS(t)$ is so negative that all model snow layers are compacted and densified to ρ_{max}, but still $HS^* > HS_{\mathrm{obs}}(t)$ the *Runoff submodule* is activated and runoff $R(t)$ is defined as $R(t) = (HS^* - HS_{\mathrm{obs}}(t)) \cdot \rho_{\mathrm{max}}$.

All layer thicknesses are cut by a respective portion: $(HS^* - HS_{\mathrm{obs}}) \cdot \frac{hs_i^*}{HS^*}$. This mechanism does not reduce total number of layers, but layers potentially get very thin. During the melt season, where most of the runoff is produced, the *Runoff submodule* is more or less continuously active until $HS_{\mathrm{obs}}(t) = 0$ and all the snow has been converted to runoff. For a distinct snowpack from the first snowfall (t_1) until getting snow-free again (t_2) one has $\sum_{t_1}^{t_2} R(t) = SWE_{\mathrm{pk}}$.

In Fig. 1 the *Drenching module* is shown by the brown and its *Runoff submodule* by the green arrows.

2.3 Calibration

ΔSNOW has seven parameters that have to be calibrated: ρ_0, ρ_{max}, η_0, k, τ, c_{ov}, and k_{ov} (cf. Table 3). For the first four parameters one finds suggestions and ranges in the literature:

Sturm and Holmgren (1998) do not address the criticality for the choice of new snow density, however, they use constant $\rho_0 = 75\,\mathrm{kg\,m^{-3}}$. It is a well known characteristic of new snow to show large variations in densities. Helfricht et al. (2018) reviewed many studies and give a general range of $10 - 350\,\mathrm{kg\,m^{-3}}$, narrowing it down to "mean values" between $70 - 110\,\mathrm{kg\,m^{-3}}$. Note, that this is daily densities. Sub-daily means of new snow densities are lower. Helfricht et al. (2018), for example, come up with an average of $68\,\mathrm{kg\,m^{-3}}$ for hourly time intervals. During the calibration process for the ΔSNOW model ρ_0 was varied from 50 to $200\,\mathrm{kg\,m^{-3}}$.

The second density-related calibration parameter is ρ_{max}, the maximum possible density within the model framework. Rohrer and Braun (1994) set such a maximum at $450\,\mathrm{kg\,m^{-3}}$. Sturm et al. (2010) defined it for five different climate classes, ranging from 217 to $598\,\mathrm{kg\,m^{-3}}$. Glaciologists consider the density at which snow transitions to firn to span 400 to $800\,\mathrm{kg\,m^{-3}}$ (e.g., Cuffey and Paterson, 2010). Still, manual density measurements of seasonal snow used in previous studies hardly ever exceed $500\,\mathrm{kg\,m^{-3}}$ (e.g., Jonas et al., 2009; Guyennon et al., 2019). Armstrong and Brun (2010) limit it to approximately 400 to $500\,\mathrm{kg\,m^{-3}}$ too. In order to find the best value for ρ_{max} used in ΔSNOW, it was varied from 300 to $600\,\mathrm{kg\,m^{-3}}$.

Equation (2) needs η_0, the "viscosity at [which] ρ equals zero" (Sturm and Holmgren, 1998). It is found to be in the order of $8.5 \times 10^6\,\mathrm{Pa\,s}$ (Sturm and Holmgren, 1998), $6 \times 10^6\,\mathrm{Pa\,s}$ (Jordan et al., 2010), and $7.62237 \times 10^6\,\mathrm{Pa\,s}$ (Vionnet et al., 2012). During the calibration process for the ΔSNOW model η_0 was varied from 1 to $20 \times 10^6\,\mathrm{Pa\,s}$. Parameter k, the second necessary parameter in Eq. (2), was varied from 0.011 to $0.08\,\mathrm{m^3\,kg^{-1}}$ by Sturm and Holmgren (1998) depending on climate region and respective different types of snow. However, they cite Keeler (1969) in their Table 2 with values for k for "Alpine-new" snow of up to $0.185\,\mathrm{m^3\,kg^{-1}}$. In more complex snow models k is set to $0.023\,\mathrm{m^3\,kg^{-1}}$ (see Crocus: b_η in Vionnet et al. (2012)'s Equation (7); and also in Equation (2.11) of Jordan et al., 2010) or $0.021\,\mathrm{m^3\,kg^{-1}}$ (see SNTHERM: Equation (29) in Jordan, 1991). Its range for the ΔSNOW model calibration was set from 0.01 to $0.2\,\mathrm{m^3\,kg^{-1}}$.

There are no references for the latter three parameters. Threshold deviation τ, as mentioned, might be interpreted as a measure of observation error, is regarded to be in the order of a few centimeters, and was modified from $1\,\mathrm{cm}$ to $20\,\mathrm{cm}$ for calibration. The last two parameters, c_{ov} and k_{ov}, determine the role of overburden strain and are newly introduced in the ΔSNOW model. At least the limits of c_{ov} could be defined (Sect. 2.2.1) as $c_{\mathrm{ov}} \in \left[0, \min(\frac{1}{\sigma_0})\right]$. k_{ov} is only known to be a dimensionless, real, positive number. For calibrating ΔSNOW c_{ov} and k_{ov} were restrained by $[0, 10^{-3}\,\mathrm{Pa^{-1}}]$ and $[0.01, 10]$, respectively.

The calibration performed in this study is based on $\Delta t = 1\,\mathrm{d}$, but longer as well as shorter Δt are conceivable and could be handled by the ΔSNOW model too. Note, however, at least some calibration parameters will change significantly when changing Δt. This gets obvious when considering new snow density ρ_0, which of course is different if defined for one hour or for a three day timestep. The usage of this publication's calibration parameters can, therefore, only be suggested for daily snow depth records.

2.3.1 Calibration data and method

The calibration process needs SWE data, which are quite rare per se (see Sect. 1), and regular snow depths records from the same places. There are surprisingly few places where both parameters have been consequently observed side by side for many years, e.g., daily HS measurements accompanied by weekly, biweekly, or monthly SWE measurements.

Gruber (2014) collected 14 years of weekly SWE data from six stations in the Eastern Alps, measured by the observers of the Hydrographic Service of Tyrol (Austria) between winters 1998/99 and 2011/12. The measurements of snow depth and water equivalent were made manually in snow pits with rulers and snow sampling cylinders ($500\,\mathrm{cm^3}$), respectively. The sites range from 590 m to 1650 m altitude and are situated in relatively dry, inneralpine regions as well as in the Northern and Southern Alps, which are more humid due to orographic enhancement of precipitation (see Gruber, 2014, for details). The

sites in the Southern Alps even show a moderate maritime influence due to their vicinity to the Mediterranean Sea, the most important source of moisture for this region (e.g., Seibert et al., 2007). These $6 \times 14 = 84$ winter seasons cover 1166 measured HS–SWE pairs. Besides these SWE measurements manual HS measurements are available for every day at the respective stations. Figure A1 and Table A1 provide a map and a list, respectively.

305   The second source for SWE measurements used for calibration is Marty (2017). The Swiss SLF freely provides biweekly SWE and daily HS data from 11 stations in Switzerland. The HS measurements, accompanying the biweekly SWE measurements, were compared with the contemporary value of the daily HS records. Only those sites and years were used for calibration where the respective values of the daily HS record match the values of the biweekly measurements. If this condition is fulfilled, it is supposed that SWE and HS measurements fit together sufficiently well, although they unfortunately cannot always be taken exactly at the same place, which introduces uncertainty (e.g., López-Moreno et al., 2020). Consequently, 9 stations were used, most of them in the Northern Alps, some inneralpine, spanning an altitude range from 1200 m to 1780 m, with all in all 56 winters and 363 pairs of HS and SWE measurements. Details are given in Fig. A1 and Table A1. Other stations and years suffer from discrepancies caused by too far spatial distances between the measurements etc.

    In order to ensure an unperturbed validation, the observation data sets from Austria and Switzerland (1529 $SWE - HS$ pairs) were split in two almost equally big halves, one for model calibration (SWE_{cal}) and one for validation (SWE_{val}). The two data sources (Gruber, 2014; Marty, 2017) do not address the accuracy of the manual SWE observations. Mostly, SWE measurements made with snow sampling cylinders are used as references in comparison studies, without addressing *their* accuracy (e.g., Sturm et al., 2010; Dixon and Boon, 2012; Kinar and Pomeroy, 2015; Leppänen et al., 2018). López-Moreno et al. (2020) provide a reported range of 3-13%, and condense the results of their own experiments to an error range of 10-15% for bulk snow density. The majority of SWE_{cal} and SWE_{val} comes from the Hydrographic Service of Tyrol, Austria, where snow sampling cylinders ($500 \, \text{cm}^3$) are used (Sect. 2.3.1). The repeatability of this kind of measurement is estimated at $\pm 4\%$ for glacier mass balance studies (R. Prinz, Univ. of Innsbruck, Austria; pers. comm.). Roughly interpreting these density measurement "variabilities" as relative observation errors for SWE, the results for absolute accuracy would typically spread across the wide range of about 2 to $50 \, \text{kg} \, \text{m}^{-2}$.

325   Model calibration was performed with the statistical software R (R Core Team, 2019) and the R package *optimx* (Nash, 2014). Results were obtained with optimization methods *L-BFGS-B* (Byrd et al., 1995) followed by *bobyqa* (Powell, 2009), which both are able to handle lower and upper bounds constraints. The function to be minimized was the root mean square error (RMSE) of SWEs from the ΔSNOW model and observed SWEs, using the calibration data set SWE_{cal}.

3   Results

330 This section evaluates the ability of ΔSNOW to calculate snow water equivalents exclusively from snow depths, and its practicability. Table 3 gives an overview of all parameters and summarizes the optimal setting for ΔSNOW. A discussion of the best-fitted values and of the model sensitivity to parameter changes can be found in Sect. 4.

The minimal RMSE between all SWE observations used for calibration (SWE_{cal}) and the respective modeled values were reached for new snow density $\rho_0 = 81\,\mathrm{kg\,m^{-3}}$, maximum density $\rho_{max} = 401\,\mathrm{kg\,m^{-3}}$, viscosity parameters $\eta_0 = 8.5 \times 10^6\,\mathrm{Pa\,s}$

335   and $k = 0.030\,\mathrm{m^3\,kg^{-1}}$, threshold deviation $\tau = 2.4\,\mathrm{cm}$, and overburden parameters $c_{ov} = 5.1 \times 10^{-4}\,\mathrm{Pa^{-1}}$ and $k_{ov} = 0.38$.

3.1 Validation and comparison to other models

In this study no quantitative comparison with thermodynamic snow models was performed, since they need further meteorological data and the focus was on data records constrained to snow depths. However, the ΔSNOW model was thoroughly evaluated against ERMs. Figure 2 and Table 4 show the results. Even though ERMs do not need meteorological data, it is not

340   straightforward to calibrate them for new sites and applications. From the vast number of ERMs (cf. Avanzi et al., 2015) the ones of Pistocchi (2016) and Guyennon et al. (2019) were chosen to be fitted to SWE_{cal}. These models are quite new and easy to calibrate. Additionally, an approach simply using a constant bulk snow density at every point in time was calibrated to fit this study's data. $278\,\mathrm{kg\,m^{-3}}$ turned out to be the optimal value minimizing root mean square errors of all SWE_{cal} values. Moreover, Jonas et al. (2009) and Sturm et al. (2010) were used for comparison. Unfortunately, calibration of these powerful models

345   would have needed much more data than the 780 SWE-HS-pairs of the SWE_{cal} data set. Therefore, Jonas et al. (2009) and Sturm et al. (2010) were used with their standard parameters, but for Jonas et al. (2009) it was distinguished between regions (see Fig. 2's caption). Other contemporary approaches had to be ignored, mostly because of the problematic transferability of regional parameters (e.g., McCreight and Small, 2014, or Mizukami and Perica, 2008).

The bias of modeled SWE (lower left panel in Fig. 2) is quite low and tends to be positive, meaning SWE is often slightly

350   overestimated by the ERMs. ΔSNOW slightly underestimates SWE on average, with a median bias of $-3.0\,\mathrm{kg\,m^{-2}}$. The overall good results for the ERMs is not surprising, since they are dedicated to perform well on average. The specially calibrated versions of Pistocchi (2016) and Guyennon et al. (2019) show a significantly smaller bias than their originals. The model of Jonas et al. (2009) has the smallest bias for their "Region 7", encompassing the dry, inneralpine Engadin as well as parts of the Southern Alps and the very East of Switzerland (Samnaun), which is partly influenced by orographic precipitation from

355   Northwesterly flows. In terms of heterogeneity in precipitation climate "Region 7" is comparable to the region where the SWE data of this study comes from.

The other three indicators illustrated in Fig. 2 and summarized in Table 4 show the improved performance of ΔSNOW compared to ERMs: The latter are intrinsically tied to snow depth (see Sect. 1.2) and are systematically forced to overestimate SWE_{pk}. Note, the maximal SWE of a winter season does not necessarily equal the highest measured SWE, because measure-

360   ments are only taken weekly or biweekly. In the vast majority of the SWE records used for this study, the highest seasonal observation is followed by at least one lower SWE reading. Sometimes real SWE might be higher after the highest measurement of a winter season was taken, but a thorough data check revealed, this is of minor importance here. It is sufficiently precise to assume that measured seasonal maximum SWE equals SWE_{pk}. ΔSNOW's bias of SWE_{pk} is very minor, only $+0.3\,\mathrm{kg\,m^{-2}}$. Moreover, the ΔSNOW model works better for the timing of SWE_{pk} (not shown in Fig. 2 and Table 4). ERMs tend to model

365   SWE_{pk} some days too early, because the date of modeled SWE_{pk} is shifted towards the date of highest HS (cf. Fig. 4).

Another satisfactory validation result for Δsnow is shown in Fig. 2's upper panels. RMSEs for all SWE values are constantly lower than if modeled with ERMs: a RMSE of $30.8\,\mathrm{kg\,m^{-2}}$ (Δsnow) contrasts RMSEs between 39.1 and $50.9\,\mathrm{kg\,m^{-2}}$ (ERMs). Calibrating the models of Pistocchi (2016) and Guyennon et al. (2019) results in some improvement, at least they perform much better than the "constant density approach" after the calibration. The model of Jonas et al. (2009) does a de-

370   cent job even without recalibration. Sturm et al. (2010)'s method is calibrated with data from the Rocky Mountains. For this comparison the "alpine" parameters of Sturm et al. (2010) were taken, however, conditions might differ too much from the European Alps. Absolute errors in SWE increase with increasing SWE. For snowpacks lighter than $75\,\mathrm{kg\,m^{-2}}$ Δsnow's RMSE is $17\,\mathrm{kg\,m^{-2}}$, between $75\,\mathrm{kg\,m^{-2}}$ and $150\,\mathrm{kg\,m^{-2}}$ it is $26\,\mathrm{kg\,m^{-2}}$, and for snowpacks heavier than $150\,\mathrm{kg\,m^{-2}}$ it increases to $43\,\mathrm{kg\,m^{-2}}$.

375   The Δsnow model also has a small RMSE of $36.3\,\mathrm{kg\,m^{-2}}$ when modeling SWE_pk (Fig. 2, upper right; Table 4, last two columns). Also the SWE_pk-RMSEs for the different SWE classes are very close to those for SWE, which emphasizes Δsnow's ability to model all individual SWEs comparably well. The evaluated ERMs have much higher, mostly at least doubled errors in simulated SWE_pk. Remarkably, the simple ρ_{278} approach performs relatively well. In case the Jonas et al. (2009) model is suitably adjusted to regional specialties, it performs better than the other ERMs, but still significantly worse

380   than Δsnow.

These results demonstrate that Δsnow outperforms ERMs. This can be argued on base of Fig. 2, but even more when looking at the ERM studies themselves: Jonas et al. (2009) provide RMSEs between 50.9 and $53.2\,\mathrm{kg\,m^{-2}}$ for their standard model, which are quite high values compared to the findings of the study in hand ($39.4\,\mathrm{kg\,m^{-2}}$ for their Region 7, see Table 4). One explanation could be that Jonas et al. (2009) as well as other ERM studies rely on a huge amount of, but still diverse mea-

385   surements in terms of record length, observations per season etc. The Δsnow model study only consists of data from selected stations with long and regular SWE readings, where also ERMs seem to work better. Guyennon et al. (2019) summarize their and other studies' validation results using MAE, the mean absolute error. Sturm et al. (2010) assess the bias for their "alpine" model at $+29\,\mathrm{kg\,m^{-2}}$ with a standard deviation of $57\,\mathrm{kg\,m^{-2}}$, and they outline that "in a test against extensive Canadian data, 90% of the computed SWE values fell within $\pm80\,\mathrm{kg\,m^{-2}}$ of measured values". Table 4 provides an overview and shows, that

390   ERMs generally perform better with this study's data than with their original data.

3.2   Illustration

Figure 1 schematically shows the functioning of the Δsnow model. A practical example is provided in Fig. 3, based on the optimal calibration parameters found during this study. Kössen, the station shown, is situated in the Northern Alps at $590\,\mathrm{m}$ above sea level (cf. Fig. A1). Although it is a low-lying place it is known to be snowy, which is, firstly, due to intense orographic

395   enhancement of precipitation associated with Northwesterly to Northeasterly flows in the respective region (Wastl, 2008) and, secondly, comparably frequent inflow of cold continental air masses from Northeast. Showing the example of Kössen should emphasize the versatile usability of Δsnow: It is not only designed for high areas with deep, long-lasting snowpacks, but also for valleys with shallow, ephemeral snowpacks. Winter 2008/09 was chosen because Δsnow shows a rather typical

performance in terms of RMSE and BIAS in Kössen (see Table 4, values in brackets) and because some important, model-intrinsic features can be addressed and discussed:

Late November 2008 brought the first, however transient snowpack of the season (Fig. 3). The ΔSNOW model identifies two days with snowfall (purple markings) and models two respective snow layers, which can be distinguished by the thin black line in Fig. 3. After about a week the snowpack starts to melt, the snow layers reach ρ_{max} very fast (the blue shading gets dark), and finally all the snow was converted to runoff (green markings). In the second half of December there were three days with new snow, followed by a strong decline in snow depth. In the frame of the ΔSNOW model this HS decrease is only possible, if the layers "get wet" and the *Drenching module* is activated (marked in brown). The layers get denser, starting at the top. However, the decrease was "manageable" only by increasing the two uppermost layer densities to ρ_{max} and making the third layer just a bit denser. Not all layers got to ρ_{max} and no runoff was modeled. The ΔSNOW model conserves the two dense layers until the end of the winter, which can clearly be seen in Fig. 3. One could interpret the layers as consisting of melt forms or a refrozen crust. However, such interpretations require caution, because modeling detailed layer features is not the intention of ΔSNOW. During January Fig. 3 shows a phase where modeled values and observations agree to a high extent and only the *Scaling module* is activated for small adjustments (white markings). Small "stretching events" can be recognized, e.g. on January 2nd and 3rd, where model snow layers are set less dense in order to avoid too frequent mass gains. During continuous snowfalls in February the successive darkening of the blue layer shadings illustrates a phase of consequent compaction, which actually lasts until March, when strong decreases in HS_{obs} start to activate the *Drenching module*. Still, runoff is not yet produced. Only in the second half of March does the whole model-snowpack reach ρ_{max} ("saturation"). The ablation phase is clearly distinguishable and lets the snowpack vanish rapidly towards April 10th, 2009.

The snow depth record of Kössen from 2008/09 was also used to compare different ERMs and ΔSNOW to SWE observations (Fig. 4). These measurements (light blue circles) are part of the SWE_{val} sample and were manually made with snow sampling cylinders; one after the December 2008 snowfall, and another nine on a nearly weekly base between late January and late March 2009. Figure 4 also provides various model results and some respective key values are given in Table 4. Not surprisingly, thus evidently, the ERMs' SWE curves follow the snow depth curve (black dashed line). The first four measurements are not well simulated by the ΔSNOW model (red line), the ERMs perform better in this illustrative case. But after the stronger snowfalls of February the picture changes indisputably in favor of the ΔSNOW model. This is a typical pattern, because ERMs are too strongly tied to snow depth and, therefore, mostly (1) overestimate SWE_{pk}, (2) model its occurrence too early, and (3) – most importantly – force modeled SWE to reduce during pure compaction phases after snowfalls. Evidently, the ability of ΔSNOW to conserve mass during the phases with dry metamorphism is its strongest point, not only in Kössen 2008/09 but also on average (cf. Fig. 2 and Table 4).

4 Discussion and outlook

430 Model results clearly depend on the parameters. Their optimal values are subject to calibration. The choice of the best-fitted values is rated and discussed in the following Sects. 4.1 to 4.5. Sections 4.6 to 4.8 cover possible future developments, accuracy issues, and ΔSNOW's applicability in remote sensing.

4.1 New snow density ρ_0

Being aware of both, the potentially large variations of new snow density and the possible cruciality of this parameter for 435 SWE simulation by the ΔSNOW model, ρ_0 was chosen to be a constant in the framework of the model. $\rho_0 = 81 \, \text{kg m}^{-3}$ turned out to be the best choice after calibration with SWE_{cal}. This value clearly lies within the broader frame of possible new snow densities (Table 3) and quite closely to Sturm and Holmgren (1998)'s $75 \, \text{kg m}^{-3}$, but it is found in the lower part for typical new snow densities (e.g., Helfricht et al., 2018). A possible explanation is that the SWE measurement records used for the calibration tend to underrepresent late winter and spring conditions. Regular (weekly, biweekly) observations capture 440 the short melt seasons worse than the longer accumulation phases. Therefore, SWE records might be biased towards early and mid winter new snow densities, which are lower (e.g., Jonas et al., 2009). Still, there are also some indications that using, e.g., $100 \, \text{kg m}^{-3}$ as constant new snow density when modeling SWE results in an overestimation of precipitation (up to 30% according to Mair et al., 2016). The calibrated value for ρ_0 can be regarded as a reasonable result, even more when only considering it as a model parameter but not as a physical constant.

445 The sensitivity analysis illustrated in Fig. 5 confirms the importance of a good choice of ρ_0. Increasing ρ_0 leads to a decrease of the relative bias of seasonal SWE maxima (SWE_{pk}). Note the definition of the relative bias in Fig. 5's caption. In absolute values: too small ρ_0 cause too small SWE_{pk}, while using higher values leads to an overestimation of SWE_{pk}. This behavior supports the above-mentioned tendency to overestimate precipitation when choosing constant $100 \, \text{kg m}^{-3}$ as new snow density. As expected, the new snow density is the most crucial parameter of the ΔSNOW model (cf. Table 3). The median relative bias 450 of SWE_{pk} changes by -0.46% per $+1 \, \text{kg m}^{-3}$, if the whole calibration range of ρ_0 is considered to calculate the sensitivity $(50 - 200 \, \text{kg m}^{-3})$. This means a median change in SWE_{pk} of $+0.37 \, \text{kg m}^{-2}$ when ρ_0 is risen by $+1 \, \text{kg m}^{-3}$. If the limits are restricted more tightly around the optimal value, the gradient is even steeper: -0.62% and $+0.50 \, \text{kg m}^{-2}$ per $+1 \, \text{kg m}^{-3}$, respectively, when the gradient is approximated for the range $70 - 90 \, \text{kg m}^{-3}$. The widely-used ρ_0 value of $100 \, \text{kg m}^{-3}$, consequently, causes a median overestimation of SWE_{pk} of about 12% in the ΔSNOW model. Daily SWE shows the same 455 behavior (not shown) and users should be aware of this. The suggestion is to either use the best-fitted parameters of this study or recalibrate *all* parameters with appropriate SWE data, but not to adjust only single parameters. The value of $\rho_0 = 81 \, \text{kg m}^{-3}$ seems to be a good compromise, at least in alpine areas. However, for very maritime, very dry, polar or tundra regions the optimized ρ_0 should be used with caution.

4.2 Maximum density ρ_{max}

The maximum bulk snow density of a snowpack changes from year to year and site to site. For ΔSNOW simplicity and independence from meteorological variables outweigh precision. Even more so, when there are good arguments for the existence of a typical maximum bulk density ρ_{max}. Put simply, seasonal and also ephemeral snowpacks melt away when they get water saturated. Before that, there is limited time for dry densification; dry winter snow's bulk density is widely described as staying below about $350\,\mathrm{kg\,m^{-3}}$ (e.g., Cuffey and Paterson, 2010; Sandells et al., 2012). Accounting for the fact that volumetric liquid water content of about 10% marks the funicular mode of liquid distribution in old, coarse-grained snow (Denoth, 1982; Mitterer et al., 2011), this leads to the rough estimate of a typical maximum bulk density of about $\frac{9}{10}\cdot 350 + \frac{1}{10}\cdot 1000 = 415\,\mathrm{kg\,m^{-3}}$. Convincingly, the optimal value for ρ_{max} in the ΔSNOW model turns out to be $401\,\mathrm{kg\,m^{-3}}$, which is close to that value and well within the range given in the literature (Table 3). Moreover, this is virtually the same as the median maximum seasonal density of the SWE_{val} data records ($400\,\mathrm{kg\,m^{-3}}$, see box plot in Fig. 6), another indication why ρ_{max} could be regarded as a typical seasonal maximum of ρ_{b}.

Figure 5 illustrates the similarity between ρ_0 and ρ_{max} regarding their influence on SWE simulations. Keeping the other six ΔSNOW parameters constant but increasing ρ_{max} leads to increased SWE_{pk} and vice versa – just like ρ_0. The ΔSNOW model is not as sensitive to changes in ρ_{max} as it is to changes in ρ_0: Raising ρ_{max} by $+1\,\mathrm{kg\,m^{-3}}$ leads to a mean decrease of the relative bias of SWE_{pk} of -0.06%, which corresponds to an increase in absolute SWE_{pk} of $+0.24\,\mathrm{kg\,m^{-2}}$ per $+1\,\mathrm{kg\,m^{-3}}$. We consider the ρ_{max} value of $401\,\mathrm{kg\,m^{-3}}$ to be representative for Alpine areas as our calibration dataset encompasses the full range of environmental conditions. Be aware that solely changing parameter ρ_{max} for an application of the ΔSNOW model elsewhere, without proper recalibration of the other parameters, might lead to significant changes in the results for SWE.

4.3 Viscosity parameters η_0 and k

Equation (2) represents the settlement and densification function of ΔSNOW. Two parameters η_0 and k act as adjustment screws and have to be calibrated. In this study best-fitted η_0 is $8.5 \times 10^6\,\mathrm{Pa\,s}$ and the optimized value for k is $0.030\,\mathrm{m^3\,kg^{-1}}$. Both values are close to other studies' results and suggestions (Table 3).

As far as ΔSNOW's sensitivity to changes in the viscosity parameters η_0 and k is concerned, Fig. 5 shows that an isolated rise of the model snow viscosity – either by enhancing η_0 or k – increases the relative bias of SWE_{pk}, which means a decrease in absolute values of SWE_{pk}. This behavior is consistent, since higher viscosity reduces the densification rate and the model-snowpack tendentially stays deeper. Consequently, increases in observed snow depth tend to bring less new snow while the *New Snow module* is run (Sect. 2.2.1). Finally, simulated SWE_{pk} is reduced when η_0 or k are increased and vice versa.

4.4 Threshold deviation τ

ΔSNOW's parameter to cope with uncertainties in snow depth is τ, and it is considered to be not more than a few centimeters. In particular, it should avoid excessive production of snow mass in the model through too frequent simulation of new snow events (see Sect. 2.2). τ is kind of a peculiarity of the ΔSNOW model and therefore no bounds can be found in literature. It was

generously accepted to range between 1 and $20\,\mathrm{cm}$ for calibration and turned out to be optimal at $\tau = 2.4\,\mathrm{cm}$ (Table 3). Given the wide range of possible values, this is very close to what it would be expected to be as a measure for HS_{obs} accuracy.

Model sensitivity to changes in τ turns out to be quite low for values in the order of a few centimeters, but the influence on simulated SWE_{pk} is strongly increasing if τ is chosen greater than about $5\,\mathrm{cm}$ (Fig. 5). This result makes a lot of sense, if τ is seen as a measure of observation accuracy, because this is very likely to be better than $5\,\mathrm{cm}$. Like changes in η_0 and k, changes in τ are indirect proportional to changes in SWE_{pk}, for a closely related reason: The bigger τ the more often small new snow events are not counted as such because the *Scaling module* (Sect. 2.2.2) is more frequently activated at the cost of the *New Snow module* (Sect. 2.2.1).

4.5 Overburden parameters c_{ov} and k_{ov}

Aside from τ, there are two more parameters that are peculiar to the ΔSNOW model. They are needed to simulate unsteady compaction by overburden load of new snow. Because of their presumed uniqueness in the snow model spectrum there is no information available on how to choose them (see Sect. 2.3). The calibration produces $c_{\mathrm{ov}} = 5.1 \times 10^{-4}\,\mathrm{Pa}^{-1}$ and $k_{\mathrm{ov}} = 0.38$ as best-fitted values (Table 3).

The sensitivity of modeled SWE_{pk} to changes in either c_{ov} or k_{ov} are quite minor. (See Fig. 5 for c_{ov}. k_{ov} is not shown, because it is comparable, but of opposite sign.) The reason for this relative insensitivity of the model to changes in c_{ov} and k_{ov} could be the contradicting effects of these two overburden parameters: Higher c_{ov} lead to higher SWE and SWE_{pk}, higher values of k_{ov} cause lower SWE.

4.6 Incorporating rain-on-snow and other possible improvements

In principle, ΔSNOW could deal with rain-on-snow events. Unsteady compaction due to overburden load, for example, is not restricted to new snow. It could also be triggered by the mass of rain water, both in nature, and in the framework of the ΔSNOW model. Still, the respective feature is not implemented at the moment, because identifying criteria for rain-on-snow events based on pure snow depth records is very problematic, and beyond the scope of this paper.

Another eventual future development is the refinement of the density parameters ρ_0 and ρ_{max} since, firstly, ΔSNOW reacts quite sensitively to their changes and, secondly, some relations are well known, e.g., ρ_0's dependence on the climatic aridity or ρ_{max}'s tendency to increase for aging snow. Setting ρ_{max} to a fixed value of $401\,\mathrm{kg\,m^{-3}}$ actually disqualifies the ΔSNOW model for snow older than estimated 200 days. Additional calibrations could be performed for very maritime, very dry, polar, or tundra regions as well as for very long-lasting snowpacks. Note, however, all of these adaptions introduce more parameters to the ΔSNOW model and reduce its generality. Benefits should be evaluated critically, and probably this evaluation should start with the overburden load treatment of ΔSNOW. It is possible that refining the density parameters is more valuable than the special treatment of unsteady compaction due to overburden loads.

4.7 *SWE* accuracy

Table 4 provides an overview of uncertainties for SWE, also for thermodynamic models: Vionnet et al. (2012) find a RMSE and bias of $39.7 \, \mathrm{kg \, m^{-2}}$ and $-17.3 \, \mathrm{kg \, m^{-2}}$, respectively, comparing 1722 manual samplings at Col de Porte (Chartreuse Mountains, France) and Crocus. Wever et al. (2015) and Sandells et al. (2012) come up with RMSEs of about $39.5 \, \mathrm{kg \, m^{-2}}$ (SNOWPACK) and $30 - 49 \, \mathrm{kg \, m^{-2}}$ (SNOBAL), respectively. Langlois et al. (2009) find more optimistic values, however, based on much fewer data. On the contrary, Egli et al. (2009) give reason to expect higher RMSEs, but their study exclusively bases on data from the snowy, high altitude station Weissfluhjoch (Switzerland), which intrinsically promotes higher absolute errors. Essery et al. (2013)'s comprehensive simulation experiment results in a RMSE-range of $23 - 77 \, \mathrm{kg \, m^{-2}}$.

As a synopsis of the study in hand, absolute SWE accuracies could be estimated as follows: (1) 2 to $50 \, \mathrm{kg \, m^{-2}}$ for manual measurements, which are widely used as reference, (2) 30 to $40 \, \mathrm{kg \, m^{-2}}$ for thermodynamic models, and (3) 40 to $50 \, \mathrm{kg \, m^{-2}}$ for empirical regression models. In this respect, it is striking to find ΔSNOW's RMSE at $30.8 \, \mathrm{kg \, m^{-2}}$.

4.8 Application to remote sensing data

Looking at current developments in deriving SWE from snow depths monitored with lidar and photogrammetry, ΔSNOW might be considered as one of the "potential [...] other snow density models" (Smyth et al., 2019) that could be included in respective future research. Lidar and photogrammetry have errors in the order of $10 \, \mathrm{cm}$ (Smyth et al., 2019), typically corresponding to SWE errors of 20 to $40 \, \mathrm{kg \, m^{-2}}$. This is in the order of the ΔSNOW model errors. Remote sensing derived snow depth data are discontinuous through time, but ΔSNOW could be adapted for that in order to upgrade from a point model to a computationally fast distributed model. A possible combination of ΔSNOW with modern, large scale snow depth products like those presented by Lievens et al. (2019) motivates future developments in this direction.

5 Conclusions

A new method to simulate snow water equivalents (SWEs) is presented. It exclusively needs snow depths and their temporal changes as input, which, given the nature of available data, is its major advantage compared to many other snow models. It is shown that basic snow physics, implemented in a layer model, suffice to better calculate SWE than snow models relying on empirical regressions.

Regular snow depth records are used to stepwise model the evolution of seasonal snowpacks, focusing on their mass (i.e. SWE) and respective load. Snow compaction is assumed to follow Newtonian viscosity, unsteady stress for underlying snow layers by the overburden load of new snow is regarded separately, melted mass is distributed from upper to lower layers, and – eponymous for the model – the measured change in snow depth between two observations is used as a precious corrective, though by accounting for measurement uncertainties.

The ΔSNOW model mainly draws on Martinec and Rango (1991) and Sturm and Holmgren (1998), and transforms them to an open source R-code, which is available through https://cran.r-project.org/package=nixmass. ΔSNOW requires only HS

as input and doesn't need meteorological or geographical forcing, although calibration of seven parameters is needed. To provide an optimal setting and utmost applicability, data from 14 climatologically different places in the Swiss and Austrian Alps are utilized. This is challenging, since calibration needs multi-year SWE observations as well as consecutive (e.g. daily) snow depth readings from the same places. ΔSNOW is calibrated with 67 winters. The validation data set consists of another 71 independent winters. Whereas calibration is quite complex, the application of the ΔSNOW model is cheap in terms of computational effort: Deriving a one-year SWE record from 365 snow depth values, e.g., only takes a few seconds with today's standard desktop CPUs and can certainly be speeded up significantly.

In this study it is argued that ΔSNOW is situated between sophisticated "thermodynamic snow models", necessitating meteorological and other inputs, and modest "empirical regression models" (ERMs), relying on simple statistical relations between SWE and snow depth, date, altitude, and region. The key qualities of the ΔSNOW model are:

- low complexity: ΔSNOW is a semi-empirical multi-layer model with seven parameters. In some respect it is even less demanding than ERMs, because no information on date, altitude, or region is required.

- high universality: ΔSNOW simulates individual SWE values – like the important seasonal maximum SWE_{pk} – comparably well as SWE averages.

- high accuracy: ΔSNOW's performance in modeling SWE and SWE_{pk} is comparable to thermodynamic models and superior to ERMs. Root mean square errors for SWE_{pk} are $36.3\,\mathrm{kg\,m^{-2}}$ for ΔSNOW and about 70 to $> 100\,\mathrm{kg\,m^{-2}}$ for ERMs.

As the development of the ΔSNOW model is application-driven, it provides no new findings in snow physics. Still, ΔSNOW takes well known basic snow principles and arranges them in a physically consistent way, while retaining the simplicity of using the single forcing parameter of snow depth. After calibration, the ΔSNOW model is widely usable, and particularly of value for attributing snow water equivalents to all longterm and historic snow depth records, which are so valuable for climatological studies and extreme value analysis for risk assessment of natural hazards .

Code availability. R-code of ΔSNOW and some empirical regression models: https://cran.r-project.org/package=nixmass. Phyton-code of ΔSNOW, ported by M. Theurl (Univ. of Graz, Austria): https://bitbucket.org/atraxoo/snow_to_swe.

Appendix A

A map with the stations used for calibration and validation of the ΔSNOW model is shown in Fig. A1. Table A1 provides details on the stations and the data.

Appendix B

The *Scaling module* (Sect. 2.2.2) recalculates the viscosity parameter η_0. This temporary $\eta_0^*(i,t)$ does not only depend on the point in time t whenever the *Scaling module* is activated, but is also different for each layer i. The reason is described in the following.

The *Scaling module* aims for the condition, that the actual model snow depth $HS(t)$ equals the actual observed snow depth $HS_{\mathrm{obs}}(t)$.

$$HS(t) = \sum_{i=1}^{ly(t)} hs(i,t) \overset{!}{=} HS_{\mathrm{obs}}(t)$$

It follows from Eq. (2) and substituting $x(i,t) = \Delta t \cdot \widehat{\sigma}(i,t) \cdot e^{-k \cdot \rho(i,t)}$:

$$\sum_{i=1}^{ly(t)} hs(i,t) = \sum_{i=1}^{ly(t)} \frac{\eta_0^*(t) \cdot hs(i,t-1)}{\eta_0^*(t) + x(i,t)} \overset{!}{=} HS_{\mathrm{obs}}(t), \tag{B1}$$

which is a rational function f of the form

$$f(\eta) = \sum_{i=1}^{N} \frac{\eta \cdot h_i}{\eta + x_i}$$

Because $f(\eta)$ has poles at $-x_1, \ldots, -x_N$, the equation $f(\eta) = HS_{\mathrm{obs}}$ has multiple solutions. Consequently, this approach – with $\eta_0^*(t)$ being independent from layer i – shows a clear non-physical behavior making it necessary to calculate different $\eta_0^*(i,t)$ for each layer i based on Eq. (B1):

$$\eta_0^*(i,t) = \frac{x(i,t) \cdot hs(i,t)}{hs(i,t-1) - hs(i,t)}$$

The solution of this issue in the *Scaling module* of the ΔSNOW model bases on the assumption, that observed compaction between $t-1$ and t can be approximated linearly for each layer:

$$\frac{hs(i,t)}{hs(i,t-1)} \overset{!}{\approx} \frac{HS_{\mathrm{obs}}(t)}{HS_{\mathrm{obs}}(t-1)}$$

The layer-individual viscosities can be calculated as

$$\eta_0^*(i,t) = \frac{x(i,t) \cdot HS_{\mathrm{obs}}(t)}{HS_{\mathrm{obs}}(t-1) - HS_{\mathrm{obs}}(t)}$$

Substituting those values for η_0^* in Eq. (B1) fulfills its precondition, and the modeled equals the observed snow depth. The newly calculated $\eta_0^*(i,t)$ are different for each layer – in contrast to the fixed η_0 defined in Sect. 2.1, which is valid for the whole snowpack (outside the *Scaling module*). Note, these new viscosities are only used temporarily in the *Scaling module*. They have no analog in reality and can also have negative values, but they are mathematically sound.

Appendix C: Example of application – snow load map of Austria

In this section an example is given how the ΔSNOW model can be used to attain a map of snow loads in Austria. European Standards (e.g., European Committee for Standardization, 2015) define the "characteristic snow load" s_k as the weight of snow on the ground (which is the product of SWE and the gravitational acceleration) with an annual probability of exceedance of 0.02, i.e. a snow load that – on average – is exceeded only once within 50 years. Unfortunately, SWE is not measured on a regular basis at a reasonable number of sites in Austria (and most other countries). The ΔSNOW model, however, can provide longterm Austrian SWE series from widely available HS series, which can in turn be used for a spatial extreme value model. No other snow model is capable of this in a comparable manner, since either SWE_{pk} is poorly modeled (ERMs) or more meteorological input would be needed (thermodynamic models). Among several possibilities to spatially model snow depth extremes like max-stable processes (see e.g. Blanchet and Davison, 2011), the *smooth modeling* approach of Blanchet and Lehning (2010) can be used when marginals instead of spatial extremal dependence is in focus.

C1   Smooth modeling

Extremes following a generalized extreme value distribution (GEV; Coles, 2001) with parameters μ, σ and ξ can be modeled in space by considering linear relations for the three parameters of the form

$$\eta(x) = \alpha_0 + \sum_{k=1}^{m} \alpha_k y_k(x) \tag{C1}$$

at location x, where η denotes one of the GEV parameters, $y_1, \ldots, y_m$ are the considered covariates as smooth functions of the location, and $\alpha_0, \ldots, \alpha_m \in \mathbb{R}$ are the coefficients. Assuming spatially independent stations, the log-likelihood function then reads as

$$l = \sum_{k=1}^{K} \ell_k \left(\mu(x_k), \sigma(x_k), \xi(x_k) \right), \tag{C2}$$

where l only depends on the coefficients of the linear models for the GEV parameters. This approach was termed *smooth modeling* by Blanchet and Lehning (2010). A smooth spatial model for extreme snow depths in Austria was already presented in Schellander and Hell (2018), using longitude, latitude, altitude, and mean snow depth at 421 stations. Considering the strong correlation between snow depth and snow water equivalent, it would be natural to spatially model SWE extremes in the same manner.

C2   Fitting a spatial extreme value model

For this application 214 stations with regular snow depth observations in and tightly around Austria of the National Weather Service (ZAMG) and the Hydrological Services are used. The dataset has undergone quality control by the maintaining insti-

tutions and covers altitudes between 118 and 2290 m. The records have lengths of 43 years and cover winters from 1970/71 to 2011/2012.

In a first step the ΔSNOW model was applied to these snow depth series to achieve 214 data series of SWE across Austria. Then the linear models for the three GEV parameters according to Sect. C1 were defined via a model selection procedure. For that purpose a generalized linear regression was performed between the parameters and the covariates longitude, latitude, altitude, and mean snow depth, which were added in a stepwise manner. Using the Akaike information criterion (AIC; Akaike, 1974), the best linear model between a given full model ($\mu \sim$ all covariates) and a null model ($\mu \sim 1$) with the smallest AIC was selected. Using these models and the covariates of the 214 stations, a smooth spatial model for the yearly maxima of the SWE values was fitted.

C3 Return level map of 50-year snow load in Austria

The spatial extreme value model developed in the previous section was applied to a grid provided by the SNOWGRID climate analysis (Olefs et al., 2013). It offers the necessary covariates longitude, latitude, altitude and yearly mean snow depths from 1961 to 2016. The grid features a horizontal resolution of $1 \times 1\,\mathrm{km}$. Some minor SNOWGRID pixels have unrealistically large mean snow depth values, arising from a poor implementation of lateral snow redistribution at high altitudes (18 pixels, i.e. 0.02% with values between 5 and 65 m). They are masked for the calculation of SWE return level maps. The return level map for a return period of 50 years can be seen in Fig. A2.

As expected, due to the strong correlation of the SWE maxima with mean snow depth, the largest snow loads are located in the mountainous areas of Austria. Although the unrealistic mean snow depth values of SNOWGRID are masked, the model produces a number of 59 (0.06%) unrealistic snow load values larger than $25\,\mathrm{kN\,m^{-2}}$ in an altitude range between 1500 and 3700 m. For a model that would be seriously used e.g. in general risk assessment or structural design, this problem could possibly be tackled with a non-linear relation between SWE maxima and mean snow depth or altitude. This is, however, beyond the scope of this study. Note, that in the actual Austrian standard (Austrian Standards Institute, 2018) there are no normative snow load values defined above 1500 m altitude.

All but two locations of the Austrian SWE measurement series that were used for calibration *and* validation of the ΔSNOW model (see Sect. 2.3.1) are included in the dataset used to fit the spatial model in Sect. C2. Those two stations, Holzgau and Felbertauern with 14 years of SWE observations each, are used to qualitatively compare (1) the spatial model fitted in Sect. C2, (2) SWE extremes modeled from daily snow depths with the ΔSNOW model, and (3) extremes computed "directly" from (ca. weekly) observed SWE values. Figure A3 gives an idea of the model performance at stations Holzgau and Felbertauern (see Figs. A1 and A2 for their locations). For the lower-lying station Holzgau (1100 m) all three variants overlap very well. The 50-year return level is $4.65\,\mathrm{kN\,m^{-2}}$ for the smooth spatial model, $4.72\,\mathrm{kN\,m^{-2}}$ for ΔSNOW, and $4.8\,\mathrm{kN\,m^{-2}}$ for the observations. Note, that the latter stem from weekly observations and, therefore, not necessarily reflect the true yearly maxima, which naturally must be equal or slightly higher. By the way, the corresponding value of s_{k} from the Austrian snow load standard for Holzgau is $6.3\,\mathrm{kN\,m^{-2}}$ (Austrian Standards Institute (2018); accessible online at eHORA (2006)).

For the higher station Felbertauern (1650 m) the agreement between SWE from the ΔSNOW model and observed values is again very good. However, their GEV fits differ significantly. While the fit to the observations shows a negative shape parameter of $\xi = -0.1$, the fit to the values modeled with the ΔSNOW model gives a positive shape parameter of $\xi = 0.1$, leading to much larger return levels for higher recurrence times. It should be pointed out that the GEV fits based on ΔSNOW simulations and observations are unreliable, given the short data sample of only 14 yearly maxima. Indeed, by using a sample size of 43 years and borrowing strength from neighboring stations, the spatial model provides the best fit to observations as well as modeled SWE values. The 50-year snow load return values are $6.4\,\mathrm{kN\,m^{-2}}$ for the spatial model, $6.8\,\mathrm{kN\,m^{-2}}$ for ΔSNOW, and $5.7\,\mathrm{kN\,m^{-2}}$ for the fit to the observations. No normative value is defined for Felbertauern because it is situated higher than 1500 m (Austrian Standards Institute, 2018).

Author contributions. MW rose and led the project, structured and managed it. He was a key figure in developing and designing the snow model, and he did most of the writing. HS developed, coded and calibrated the model. He wrote the R-package and helped writing the paper, particularly the application example in the appendix. SG developed early versions of the model and its code.

Competing interests. The authors declare no competing interests.

Acknowledgements. The authors want to acknowledge T. Hell (Dept. of Mathematics, Univ. of Innsbruck, Austria) who substantially helped with the *Scaling module* (Sect. 2.2.2 and Appendix B). Thanks also go to the Hydrographic Service of Tyrol (Austria) which provided part of the data. A. Radlherr and J. Staudacher (ZAMG, Austria) is thanked for vivid discussions and early proof-reading, special thanks are given to L. Nicholson (Univ. of Innsbruck, Austria) for final proof-reading. Not least, we want to acknowledge M. Theurl and J. Abermann from the Univ. of Graz (Austria) for porting ΔSNOW's R-code to Phyton.

Financial support. This work was embedded in the project "Schneelast.Reform", funded by the Austrian Research Promotion Agency (FFG) and the Austrian Economic Chamber (WKO), in particular by their Association of the Austrian Wood Industries (FV Holzindustrie).

Review statement. This paper was edited by Markus Weiler and reviewed by three anonymous referees. The authors highly appreciate their comments and suggestions since they significantly improved the manuscript.

References

680   Akaike, H.: A new look at the statistical model identification, IEEE Transactions on Automatic Control, 19, 716–723, https://doi.org/10.1109/TAC.1974.1100705, 1974.

Armstrong, R. L. and Brun, E.: Snow and climate: physical processes, surface energy exchange and modeling, Cambridge University Press, Cambridge, 2010.

Austrian Standards Institute: ÖNORM B 1991-1-3:2018-12-01, 2018.

685   Avanzi, F., De Michele, C., and Ghezzi, A.: On the performances of empirical regressions for the estimation of bulk snow density, Geografia Fisica e Dinamica Quaternaria, pp. 105–112, https://doi.org/10.4461/GFDQ.2015.38.10, 2015.

Blanchet, J. and Davison, A.: Spatial modeling of extreme snow depth, The Annals of Applied Statistics, 5, 1699–1725, https://doi.org/10.1214/11-AOAS464SUPP, 2011.

Blanchet, J. and Lehning, M.: Mapping snow depth return levels: smooth spatial modeling versus station interpolation, Hydrology and Earth
690   System Sciences, 14, 2527–2544, https://doi.org/10.5194/hess-14-2527-2010, 2010.

Byrd, R. H., Lu, P., Nocedal, J., and Zhu, C.: A Limited Memory Algorithm for Bound Constrained Optimization, SIAM Journal on Scientific Computing, 16, 1190–1208, https://doi.org/10.1137/0916069, 1995.

Coles, S.: An introduction to statistical modeling of extreme values, Springer Series in Statistics, Springer-Verlag, London, 2001.

Cuffey, K. and Paterson, W. S. B.: The physics of glaciers, Butterworth-Heinemann/Elsevier, Burlington, MA, 4th ed edn., oCLC:
695   ocn488732494, 2010.

De Michele, C., Avanzi, F., Ghezzi, A., and Jommi, C.: Investigating the dynamics of bulk snow density in dry and wet conditions using a one-dimensional model, The Cryosphere, 7, 433–444, https://doi.org/10.5194/tc-7-433-2013, 2013.

Deems, J. S., Painter, T. H., and Finnegan, D. C.: Lidar measurement of snow depth: a review, Journal of Glaciology, 59, 467–479, https://doi.org/10.3189/2013JoG12J154, 2013.

700   Denoth, A.: The Pendular-Funicular Liquid Transition and Snow Metamorphism, Journal of Glaciology, 28, 357–364, https://doi.org/10.3189/S0022143000011692, 1982.

Dietz, A., Kuenzer, C., Gessner, U., and Dech, S.: Remote Sensing of Snow – a Review of available methods, International Journal of Remote Sensing, 33, 4094–4134, https://doi.org/10.1080/01431161.2011.640964, 2012.

Dixon, D. and Boon, S.: Comparison of the SnowHydro snow sampler with existing snow tube designs, Hydrological Processes, 26, 2555–
705   2562, https://doi.org/10.1002/hyp.9317, 2012.

Egli, L., Jonas, T., and Meister, R.: Comparison of different automatic methods for estimating snow water equivalent, Cold Regions Science and Technology, 57, 107–115, https://doi.org/https://doi.org/10.1016/j.coldregions.2009.02.008, 2009.

eHORA: Natural Hazard Overview & Risk Assessment Austria, https://hora.gv.at/, [Online; accessed 06-January-2021], 2006.

Essery, R., Morin, S., Lejeune, Y., and Ménard, C. B.: A comparison of 1701 snow models using observations from an alpine site, Advances
710   in Water Resources, 55, 131–148, https://doi.org/https://doi.org/10.1016/j.advwatres.2012.07.013, 2013.

European Committee for Standardization: EN 1991-1-3:2003/A1:2015, 2015.

Fierz, C., Armstrong, R., Durand, Y., Etchevers, P., Greene, E., McClung, D., Nishimura, K., Satyawali, P., and Sokratov, S.: The International Classification for Seasonal Snow on the Ground, IHP-VII Technical Documents in Hydrology, 83, http://unesdoc.unesco.org/images/0018/001864/186462e.pdf, 2009.

715   Garvelmann, J., Pohl, S., and Weiler, M.: From observation to the quantification of snow processes with a time-lapse camera network, Hydrology and Earth System Sciences, 17, 1415–1429, https://doi.org/10.5194/hess-17-1415-2013, 2013.

Goodison, B. E., Ferguson, H. L., and McKay, G. A.: Measurement and data analysis, in: Handbook of Snow: Principles, Processes, Management and Use, edited by Gray, D. M. and Male, D. H., pp. 191–274, Pergamon Press, Toronto, Canada, 1981.

Gruber, S.: Modelling snow water equivalent based on daily snow depths, Master's thesis, University of Innsbruck, 2014.

720   Guyennon, N., Valt, M., Salerno, F., Petrangeli, A. B., and Romano, E.: Estimating the snow water equivalent from snow depth measurements in the Italian Alps, Cold Regions Science and Technology, 167, https://doi.org/10.1016/j.coldregions.2019.102859, 2019.

Haberkorn, A.: European Snow Booklet – an Inventory of Snow Measurements in Europe, https://doi.org/10.16904/envidat.59, 2019.

Heilig, A., Schneebeli, M., and Eisen, O.: Upward-looking ground-penetrating radar for monitoring snowpack stratigraphy, Cold Regions Science and Technology, 59, 152–162, https://doi.org/10.1016/j.coldregions.2009.07.008, 2009.

725   Helfricht, K., Hartl, L., Koch, R., Marty, C., and Olefs, M.: Obtaining sub-daily new snow density from automated measurements in high mountain regions, Hydrology and Earth System Sciences, 22, 2655–2668, https://doi.org/10.5194/hess-22-2655-2018, 2018.

Hill, D. F., Burakowski, E. A., Crumley, R. L., Keon, J., Hu, J. M., Arendt, A. A., Wikstrom Jones, K., and Wolken, G. J.: Converting snow depth to snow water equivalent using climatological variables, The Cryosphere, 13, 1767–1784, https://doi.org/10.5194/tc-13-1767-2019, 2019.

730   Johnson, J. B., Gelvin, A. B., Duvoy, P., Schaefer, G. L., Poole, G., and Horton, G. D.: Performance characteristics of a new electronic snow water equivalent sensor in different climates, Hydrological Processes, 29, 1418–1433, https://doi.org/10.1002/hyp.10211, 2015.

Jonas, T., Marty, C., and Magnusson, J.: Estimating the snow water equivalent from snow depth measurements in the Swiss Alps, Journal of Hydrology, 378, 161–167, https://doi.org/10.1016/j.jhydrol.2009.09.021, 2009.

Jordan, R.: A One-Dimensional Temperature Model for a Snow Cover: Technical documentation for SNTHERM.89, Tech. rep., Corps of
735   Engineers, U.S. Army Cold Regions Research & Engineering Laboratory, 1991.

Jordan, R., Albert, M., and Brun, E.: Physical Processes within the snow cover and their parametrization, in: Snow and Climate: Physical Processes, Surface Energy Exchange and Modeling, pp. 12–69, Cambridge University Press, Cambridge, 2010.

Keeler, C.: Some Physical Properties of Alpine Snow, Tech. rep., Corps of Engineers, U.S. Army Cold Regions Research & Engineering Laboratory, 1969.

740   Kinar, N. J. and Pomeroy, J. W.: Measurement of the physical properties of the snowpack, Reviews of Geophysics, 53, 481–544, https://doi.org/10.1002/2015RG000481, 2015.

Koch, F., Henkel, P., Appel, F., Schmid, L., Bach, H., Lamm, M., Prasch, M., Schweizer, J., and Mauser, W.: Retrieval of Snow Water Equivalent, Liquid Water Content, and Snow Height of Dry and Wet Snow by Combining GPS Signal Attenuation and Time Delay, Water Resources Research, https://doi.org/10.1029/2018WR024431, 2019.

745   Kojima, K.: Densification of Seasonal Snow Cover, in: Physics of Snow and Ice : proceedings, vol. 1 of 2, pp. 929–952, Sapporo, Japan, http://hdl.handle.net/2115/20351, 1967.

Langlois, A., Kohn, J., Royer, A., Cliche, P., Brucker, L., Picard, G., Fily, M., Derksen, C., and Willemet, J. M.: Simulation of Snow Water Equivalent (SWE) Using Thermodynamic Snow Models in Québec, Canada, Journal of Hydrometeorology, 10, 1447–1463, https://doi.org/10.1175/2009JHM1154.1, 2009.

750   Lehning, M., Bartelt, P., Brown, R., Fierz, C., and Satyawali, P.: A physical SNOWPACK model for the Swiss Avalanche Warning Services. Part II: Snow Microstructure, Cold Regions Science and Technology, 35, 147–167, 2002.

Leppänen, L., Kontu, A., and Pulliainen, J.: Automated Measurements of Snow on the Ground in Sodankylä, Geophysica, 53, 45–64, http://www.geophysica.fi/pdf/geophysica_2018_53_leppanen.pdf, 2018.

Lievens, H., Demuzere, M., Marshall, H.-P., Reichle, R. H., Brucker, L., Brangers, I., de Rosnay, P., Dumont, M., Girotto, M., Immerzeel, W. W., Jonas, T., Kim, E. J., Koch, I., Marty, C., Saloranta, T., Schöber, J., and De Lannoy, G. J. M.: Snow depth variability in the Northern Hemisphere mountains observed from space, Nature Communications, 10, 4629, https://doi.org/10.1038/s41467-019-12566-y, 2019.

López-Moreno, J. I., Leppänen, L., Luks, B., Holko, L., Picard, G., Sanmiguel-Vallelado, A., Alonso-González, E., Finger, D. C., Arslan, A. N., Gillemot, K., Sensoy, A., Sorman, A., Ertaş, M. C., Fassnacht, S. R., Fierz, C., and Marty, C.: Intercomparison of measurements of bulk snow density and water equivalent of snow cover with snow core samplers: Instrumental bias and variability induced by observers, Hydrological Processes, 34, 3120–3133, https://doi.org/10.1002/hyp.13785, 2020.

Mair, E., Leitinger, G., Della Chiesa, S., Niedrist, G., Tappeiner, U., and Bertoldi, G.: A simple method to combine snow height and meteorological observations to estimate winter precipitation at sub-daily resolution, Hydrological Sciences Journal, 61, 2050–2060, https://doi.org/10.1080/02626667.2015.1081203, 2016.

Marks, D. G., Kimball, J. S., Tingey, D., and Link, T. E.: The Sensitivity of Snowmelt Processes to Climate Conditions and Forest Cover during Rain-on-Snow: A Case Study of the 1996 Pacific Northwest Flood, Hydrological Processes, 12, 1569–1587, 1998.

Martinec, J.: Zimni prognosy s pouzitim radioisotopu (Winter forecasts with the use of radioisotopes), Vltavska kaskada (The Vltava reservoir system), VUV Praha-Podbab, pp. 45–60, 1956.

Martinec, J.: Expected snow loads on structures from incomplete hydrological data, Journal of Glaciology, 19, 185–195, https://doi.org/10.3189/S0022143000029270, 1977.

Martinec, J. and Rango, A.: Indirect evaluation of snow reserves in mountain basins, in: Snow, Hydrology and Forests in High Alpine Areas, 205, pp. 111–120, 1991.

Marty, C.: GCOS SWE data from 11 stations in Switzerland, https://doi.org/10.16904/15, type: dataset, 2017.

McCreight, J. L. and Small, E. E.: Modeling bulk density and snow water equivalent using daily snow depth observations, The Cryosphere, 8, 521–536, https://doi.org/10.5194/tc-8-521-2014, 2014.

Mitterer, C., Hirashima, H., and Schweizer, J.: Wet-snow instabilities: comparison of measured and modelled liquid water content and snow stratigraphy, Annals of Glaciology, 52, 201–208, https://doi.org/10.3189/172756411797252077, 2011.

Mizukami, N. and Perica, S.: Spatiotemporal Characteristics of Snowpack Density in the Mountainous Regions of the Western United States, Journal of Hydrometeorology, 9, 1416–1426, https://doi.org/10.1175/2008JHM981.1, 2008.

Nash, J. C.: On Best Practice Optimization Methods in R, Journal of Statistical Software, 60, 1–14, http://www.jstatsoft.org/v60/i02/, 2014.

Olefs, M., Schöner, W., Suklitsch, M., Wittmann, C., Niedermoser, B., Neururer, A., and Wurzer, A.: SNOWGRID – A New Operational Snow Cover Model in Austria, International Snow Science Workshop Grenoble – Chamonix Mont-Blanc – October 07-11, 2013, pp. 38–45, https://arc.lib.montana.edu/snow-science/item/1785, 2013.

Painter, T. H., Berisford, D. F., Boardman, J. W., Bormann, K. J., Deems, J. S., Gehrke, F., Hedrick, A., Joyce, M., Laidlaw, R., Marks, D., Mattmann, C., McGurk, B., Ramirez, P., Richardson, M., Skiles, S. M., Seidel, F. C., and Winstral, A.: The Airborne Snow Observatory: Fusion of scanning lidar, imaging spectrometer, and physically-based modeling for mapping snow water equivalent and snow albedo, Remote Sensing of Environment, 184, 139–152, https://doi.org/10.1016/j.rse.2016.06.018, 2016.

Parajka, J., Haas, P., Kirnbauer, R., Jansa, J., and Blöschl, G.: Potential of time-lapse photography of snow for hydrological purposes at the small catchment scale, Hydrological Processes, 26, 3327–3337, https://doi.org/10.1002/hyp.8389, 2012.

Pistocchi, A.: Simple estimation of snow density in an Alpine region, Journal of Hydrology: Regional Studies, 6, 82–89, https://doi.org/10.1016/j.ejrh.2016.03.004, 2016.

Powell, M.: The BOBYQA algorithm for bound constrained optimization without derivatives, Report DAMTP 2009/NA06, University of Cambridge, https://www.nag.co.uk/IndustryArticles/bound_optimization_quadratic_approximation.pdf, 2009.

R Core Team: R: A Language and Environment for Statistical Computing, R Foundation for Statistical Computing, Vienna, Austria, https://www.R-project.org/, 2019.

Rohrer, M. and Braun, L.: Long-Term Records of Snow Cover Water Equivalent in the Swiss Alps, Nordic Hydrology, 25, 65–78, https://doi.org/10.2166/nh.1994.0020, 1994.

Sandells, M., Flerchinger, G. N., Gurney, R., and Marks, D. G.: Simulation of snow and soil water content as a basis for satellite retrievals, Hydrology Research, 43, 720–735, https://doi.org/10.2166/nh.2012.028, 2012.

Schattan, P., Köhli, M., Schrön, M., Baroni, G., and Oswald, S. E.: Sensing Area-Average Snow Water Equivalent with Cosmic-Ray Neutrons: The Influence of Fractional Snow Cover, Water Resources Research, 55, 10 796–10 812, https://doi.org/10.1029/2019WR025647, 2019.

Schellander, H. and Hell, T.: Modeling snow depth extremes in Austria, Natural Hazards, 94, 1367–1389, https://doi.org/10.1007/s11069-018-3481-y, 2018.

Seibert, P., Frank, A., and Formayer, H.: Synoptic and regional patterns of heavy precipitation in Austria, Theoretical and Applied Climatology, 87, 139–153, https://doi.org/10.1007/s00704-006-0198-8, 2007.

Smith, C. D., Kontu, A., Laffin, R., and Pomeroy, J. W.: An assessment of two automated snow water equivalent instruments during the WMO Solid Precipitation Intercomparison Experiment, The Cryosphere, 11, 101–116, https://doi.org/10.5194/tc-11-101-2017, 2017.

Smyth, E. J., Raleigh, M. S., and Small, E. E.: Particle Filter Data Assimilation of Monthly Snow Depth Observations Improves Estimation of Snow Density and SWE, Water Resources Research, 55, 1296–1311, https://doi.org/10.1029/2018WR023400, 2019.

Sturm, M. and Holmgren, J.: Differences in compaction behavior of three climate classes of snow, Annals of Glaciology, 26, 125–130, 1998.

Sturm, M., Taras, B., Liston, G. E., Derksen, C., Jonas, T., and Lea, J.: Estimating Snow Water Equivalent Using Snow Depth Data and Climate Classes, Journal of Hydrometeorology, 11, 1380–1394, https://doi.org/10.1175/2010JHM1202.1, 2010.

Valt, M., Romano, E., and Guyennon, N.: Snowcover density and snow water equivalent in the Italian Alps, in: Proceedings ISSW 2018, International Snow Science Workshop, Innsbruck, Austria, 2018.

Vionnet, V., Brun, E., Morin, S., Boone, A., Faroux, S., Le Moigne, P., Martin, E., and Willemet, J. M.: The detailed snowpack scheme Crocus and its implementation in SURFEX v7.2, Geoscientific Model Development, 5, 773–791, https://doi.org/10.5194/gmd-5-773-2012, 2012.

Wastl, C.: Klimatologische Analyse von orographisch beeinflussten Niederschlagsstrukturen im Alpenraum, Phd thesis, Ludwig-Maximilians-Universität München, http://nbn-resolving.de/urn:nbn:de:bvb:19-95453, 2008.

Wever, N., Schmid, L., Heilig, A., Eisen, O., Fierz, C., and Lehning, M.: Verification of the multi-layer SNOWPACK model with different water transport schemes, The Cryosphere, 9, 2271–2293, https://doi.org/10.5194/tc-9-2271-2015, 2015.
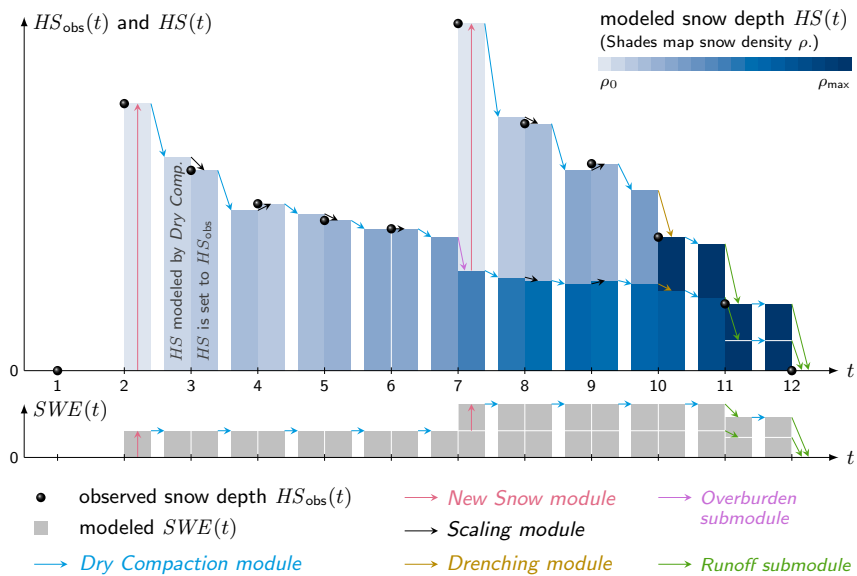
Figure 1. Schematic of ΔSNOW.
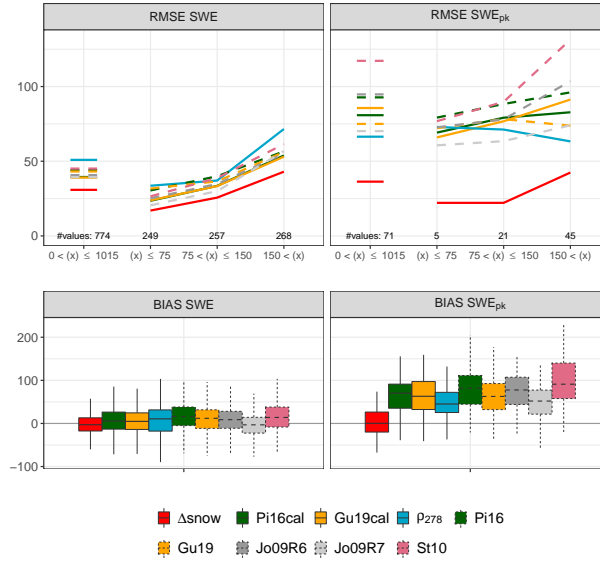
Figure 2. Root mean square errors (RMSE) and biases (BIAS) between the ΔSNOW model and different empirical regression models from the SWE_{val} observations. The ΔSNOW model, Pistocchi (2016)'s and Guyennon et al. (2019)'s models, and the "constant density approach" were calibrated with SWE_{cal} data (ΔSNOW, Pi16cal, Gu19cal, ρ_{278}; upper panels, solid lines). Dashed lines indicate the Pistocchi (2016), the Guyennon et al. (2019), the Jonas et al. (2009), and the Sturm et al. (2010) models with their standard parameters (Pi16, Gu19, Jo09R6, Jo09R7, and St10). Jo09R6 and Jo09R7 together illustrate the maximum possible spread of the Jonas et al. (2009) model since Region 6 (R6) and Region 7 (R7) are characterized by the highest and lowest "region-specific offset", respectively. The upper left panel shows RMSEs for all SWE_{val} values (short horizontal lines) as well as for three SWE classes: $SWE \leq 75$, $SWE > 150$, and intermediate. Analogously for SWE_{pk} (upper right panel). The boxes for the biases (lower panels) encompass 774 values (left panel, SWE) and 71 values (right panel, SWE_{pk}) and spread from the 25%- to the 75%-quantile, the whiskers indicate 1.5 times the interquartile range. Units are kg m^{-2}.
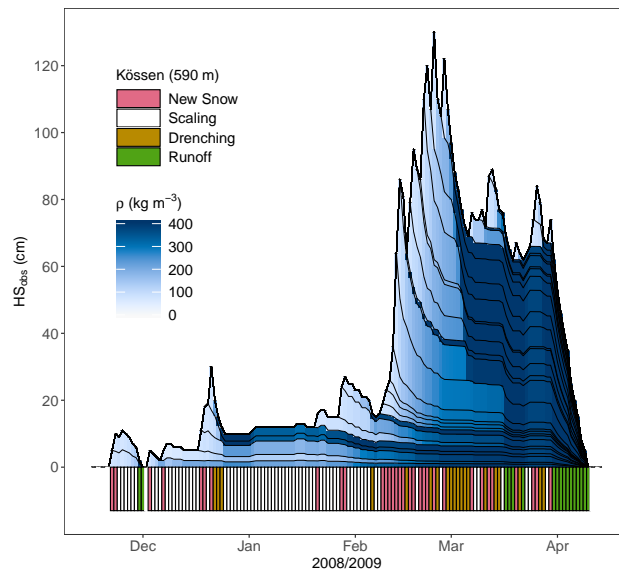
Figure 3. Winter of 2008/09 in Kössen (Northern Alps, Austria) portrays density evolution as simulated by the ΔSNOW model. Respective (sub)modules are depicted in colors at the bottom, whenever activated. Note, ΔSNOW is not intended to simulate individual layers, but to calculate daily SWE, SWE_{pk}, and daily bulk density. Descriptions and discussions of some features are given in the text.
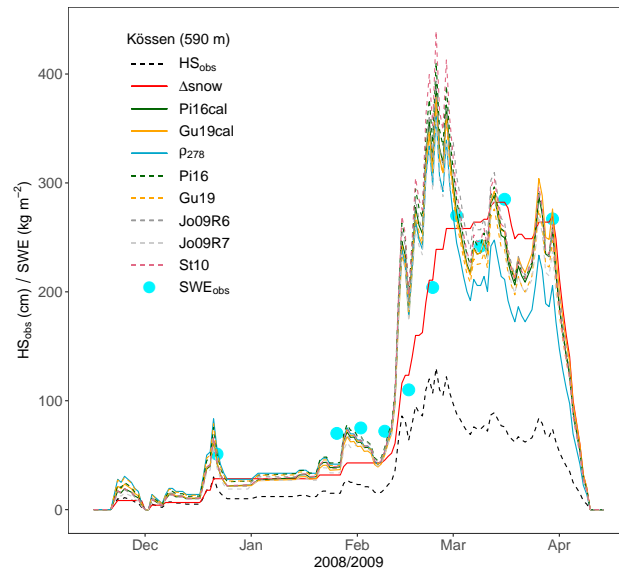
Figure 4. SWE simulations and observations (SWE_{obs}) for the winter 2008/09 in Kössen (cf. Fig. 3). Details and abbreviations are given in the text (Sect. 3.2) and summarized in Fig. 2.
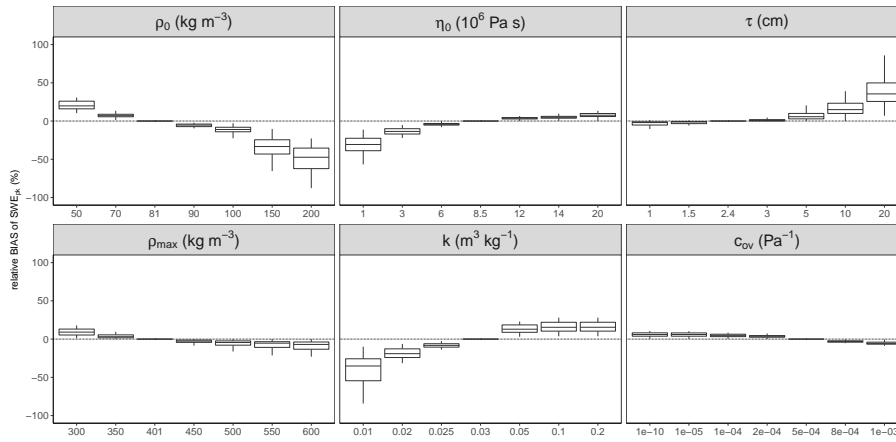
Figure 5. Sensitivity of SWE_{pk} to changes in model parameters. The "relative bias of SWE_{pk}" is defined as the difference between SWE_{pk} with best-fitted values and SWE_{pk} with changed parameters (while all others are kept unchanged), divided by the best-fitted SWE_{pk}. The boxes comprise SWE_{pk} of all stations and all years of the validation data set SWE_{val} (71 values) and display medians as well as 25% and 75% percentiles, the whiskers indicate 1.5 times the interquartile range. Details and analysis see text.
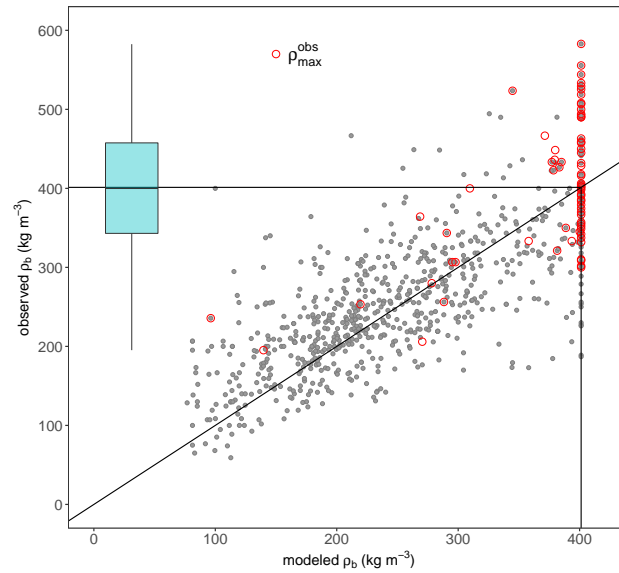
Figure 6. Scatter plot of all modeled bulk snow densities ρ_b versus all observed ρ_b from the validation data set. (SWE_{val}, 767 data pairs. Seven observations, which are higher than $600\,\mathrm{kg}\,\mathrm{m}^{-3}$, were ignored.) Red circles reflect the 71 observed yearly maxima (ρ_{max}^{obs}), most of them occur when also modeled snowpack is at $\rho_{max} = 401\,\mathrm{kg}\,\mathrm{m}^{-3}$. The box plot shows the distribution of ρ_{max}^{obs} with median, 25% and 75% percentiles, and whiskers at 1.5 times the interquartile range.

Table 1. Different types of SWE models, categorized by their essential input. TD, SE, and ERMs are abbreviations for thermodynamic, semi-empirical, and empirical regression models, respectively.

essential input	TD	SE	ERMs
HS (single values)			x
HS (regular records)	x[a]	x	
one or more atmospheric variable(s)	x		
date	x[b]		x
location parameters[c]	x[b]		x

[a]or another precipitation input

[b]only essential in some cases, e.g. for parametrizations

[c]altitude, regional climate, etc.

Table 2. Summary of compaction processes and processes forcing mass changes that are integrated in ΔSNOW, and of processes that are ignored.

module	process
New Snow	significant rise of HS, enhanced compaction due to overburden load (*Overburden submodule*)
Dry Compaction	significant decline of HS due to dry metamorphism[a] and/or deformation[a]
Drenching	significant decline of HS due to wet metamorphism[a], runoff through melt (*Runoff submodule*)
Scaling	adjustments to small changes of HS within threshold deviation τ
ignored:	snow drift compaction[a] and mass changes due to:
	rain-on-snow, runoff during snowfalls, wind drift, small snowfalls, sublimation and deposition

[a]terminology follows Jordan et al. (2010)

Table 3. The seven parameters of ΔSNOW. The last column depicts model sensitivity to changes in the density parameters. The respective gradients are means over the whole calibration ranges.

Parameter par	unit	optimal value	calibration range	literature range	sensitivity $\frac{\delta SWE_{\mathrm{pk}}\,[\mathrm{kg\,m^{-2}}]}{\delta par}$
ρ_0	$\mathrm{kg\,m^{-3}}$	**81**	50-200	75[a], 10-350 (70-110)[b]	+0.37 (+0.50[†])
ρ_{max}	$\mathrm{kg\,m^{-3}}$	**401**	300-600	450[c], 217-598[d], 400-800[e]	+0.24
η_0	$10^6\,\mathrm{Pa\,s}$	**8.5**	1-20	8.5[a], 6[f], 7.62237[g]	not calc.
k	$\mathrm{m^3\,kg^{-1}}$	**0.030**	0.01-0.2	0.011-0.08[a], 0.185[h], 0.023[f,g], 0.021[i]	not calc.
τ	cm	**2.4**	1-20	-	not calc.
c_{ov}	$10^{-4}\,\mathrm{Pa^{-1}}$	**5.1**	0-10	-	not calc.
k_{ov}	-	**0.38**	0.01-10	-	not calc.

[a]Sturm and Holmgren (1998), [b]Helfricht et al. (2018) with range for means in brackets, [c]Rohrer and Braun (1994), [d]Sturm et al. (2010), [e]Cuffey and Paterson (2010), [f]Jordan et al. (2010), [g]Vionnet et al. (2012), [h]Keeler (1969), [i]Jordan (1991). See Sect. 2.3 for more details. [†]The value in brackets is the gradient taken from the smaller window between 70 and 90 kg m^{-3} (cf. Sect. 4.1).

Table 4. Overview on SWE accuracies of different models and studies. The numbers in brackets represent the results for the example portrayed in Figs. 3 and 4 from station Kössen in 2008/09. Units are $\mathrm{kg\,m^{-2}}$, TD is short for thermodynamic snow models. Model abbreviations see caption of Fig. 2.

source	model (version)	SWE BIAS	SWE RMSE	SWE MAE	SWE_{pk} BIAS	SWE_{pk} RMSE
this study	ΔSNOW	−3.0	30.8 (21)	21.9	0.3 (−3)	36.3
	Gu19cal	4.8	39.1 (43)	27.6	63.0 (93)	85.6
	Pi16cal	5.6	39.4 (47)	28.1	70.3 (106)	80.8
	Jo09R7	−3.2	39.4 (41)	27.3	52.0 (74)	70.2
	St10	14.0	45.1 (57)	32.6	91.1 (154)	117.2
	ρ_{278}	10.6	50.9 (51)	36.3	45.2 (77)	66.4
Guyennon et al. (2019)	Gu19			49.2		
	Pi16cal			50.6		
	Jo09cal			48.5		
	St10cal			51.0		
Jonas et al. (2009)	Jo09			$50.9 - 53.2$		
Sturm et al. (2010)	St10 ("alpine")	29 ± 57				
Vionnet et al. (2012)	Crocus	−17.3	39.7			
Langlois et al. (2009)	Crocus	−7.9 to −5.4	$10.8 - 12.5$			
	SNTHERM	9 to 18.1	$18.3 - 19.3$			
	SNOWPACK	−0.1 to 5.6	$7.4 - 14.5$			
Egli et al. (2009)	SNOWPACK		56			
Wever et al. (2015)	SNOWPACK		ca. 39.5			
Sandells et al. (2012)	SNOBAL		$30 - 49$			$17 - 44$[a]
Essery et al. (2013)	various TD[b]		$23 - 77$			

[a]This is not RMSE of SWE_{pk}, but RMSE "from establishment of snowpack to SWE_{pk}". [b]See Essery et al. (2013)'s Table 10: RMSE for up to 1700 uncalibrated and calibrated simulations.
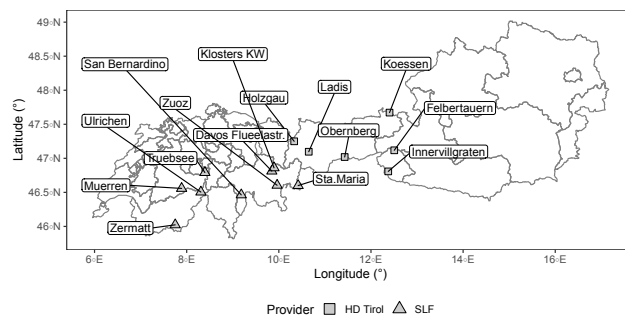
Figure A1. Locations of the stations used for calibration and validation. Austrian stations are operated by the Hydrographic Service of Tyrol (HD Tirol), the Swiss stations by the WSL Institute for Snow and Avalanche Research SLF. See Table A1 and text for more details.
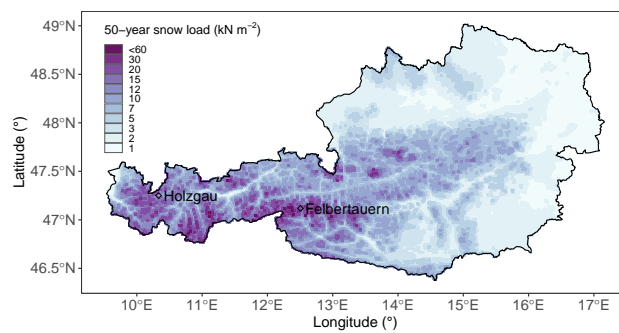
Figure A2. 50-year return levels of snow load in Austria. Two stations with SWE observations are outlined for a qualitative validation. This map bases on 214 snow depth records, ΔSNOW derived SWE, and smooth spatial modeling of their extremes.
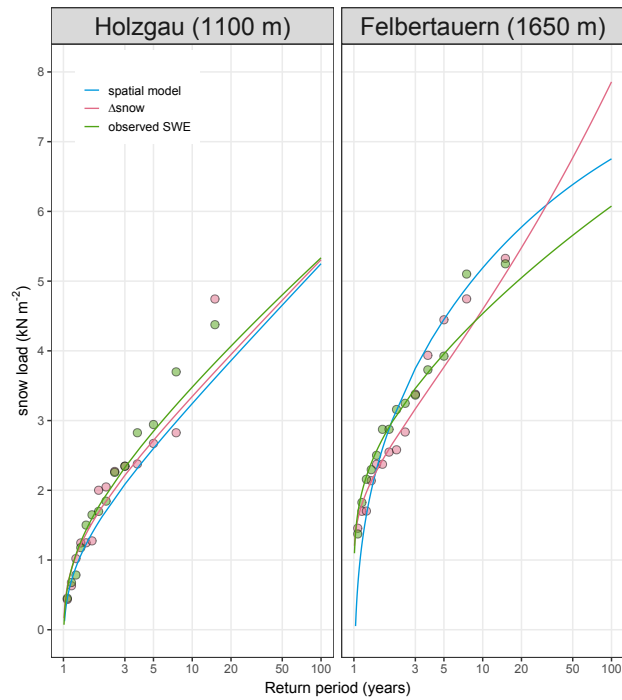
Figure A3. Return levels of snow load at stations Holzgau (left) and Felbertauern. Return periods in years are shown on the logarithmic x-axis. The blue line shows return levels obtained with the spatial extreme value model, pink bullets and lines depict yearly maxima and the GEV fit of SWE values modeled from daily snow depths with the ΔSNOW model, and green colors represent yearly SWE maxima and the corresponding GEV fit from (ca. weekly) observations.

Table A1. Overview of stations with daily snow depths record and about weekly/biweekly (Austria/Switzerland) manual SWE observations which were used for calibration and validation. $\#_{cal}^{SWE}$ and $\#_{val}^{SWE}$ give the numbers of respective manual SWE observations. Stations #1 to #6 are located in the Austrian province of Tyrol, #5 and #6 are in the sub-province of Eastern Tyrol; all operated by the Hydrographic Service of Tyrol. Swiss stations #7 to #15 are operated by the WSL Institute for Snow and Avalanche Research SLF. Compare Fig. A1. The data sources are Gruber (2014) and Marty (2017).

#	station name	lon [°]	lat [°]	alt [m]	$\#_{cal}^{SWE}$	$\#_{val}^{SWE}$	calibration seasons[a]	validation seasons[a]
1	Holzgau	10.333300	47.25000	1100	116	100	7 odd in 1999-2011	7 even in 1998-2010
2	Ladis	10.649200	47.09690	1350	83	66	7 odd in 1999-2011	6 even in 1998-2010[b]
3	Obernberg	11.429200	47.01940	1360	105	88	7 odd in 1999-2011	7 even in 1998-2010
4	Koessen	12.402800	47.67170	590	87	70	7 odd in 1999-2011	6 even in 1998-2010[b]
5	Felbertauern	12.505600	47.11810	1650	126	114	7 odd in 1999-2011	7 even in 1998-2010
6	Innervillgraten	12.375000	46.80830	1400	96	115	7 odd in 1999-2011	7 even in 1998-2010
7	Muerren	7.890193	46.55818	1650	37	27	2009,2012,2015,2017	2006,2011,2014,2016
8	Truebsee	8.395291	46.79121	1780	4	11	2016	2015,2017
9	Ulrichen	8.308283	46.50461	1350	24	23	2009,2013,2015,2017	2007,2011,2014,2016
10	Zermatt	7.751165	46.02340	1600	47	76	1961,1963 and 7 even in 2004-2016	3 even 1960-1964, 7 odd in 2005-2017
11	Davos Flueelastr.	9.848163	46.81255	1560	8	19	2012	2008,2017
12	Klosters KW	9.895973	46.86058	1200	12	22	1999	1998,2017
13	San Bernardino	9.184634	46.46326	1640	11	14	2007	2006,2014
14	Sta.Maria	10.419344	46.59981	1415	0	8	-	1969
15	Zuoz	9.962676	46.60433	1710	24	21	2011,2013,2015,2017	2006,2012,2014,2016
$\sum$					780	774	67	71

[a]Indicated years mark the start of respective winter seasons. [b]2006 is missing.